

⁵Max-Planck-Institut für Chemie, Mainz, Germany

⁶Max-Planck-Institut für Kernphysik, Heidelberg, Germany

⁷Institut für Meteorologie, Universität Leipzig, Germany

⁸Deutsches Zentrum für Luft- und Raumfahrt, Institut für Antriebstechnik, Köln, Germany

⁹Deutsches Zentrum für Luft- und Raumfahrt, Flugabteilung, Oberpfaffenhofen, Germany

Received: 20 April 2010 – Accepted: 4 May 2010 – Published: 17 May 2010

Correspondence to: C. Voigt (christiane.voigt@dlr.de)

Published by Copernicus Publications on behalf of the European Geosciences Union.

ACPD

10, 12713–12763, 2010

In situ observations of young contrails

C. Voigt et al.

Title Page

Abstract

Introduction

Conclusions

References

Tables

Figures

◀

▶

◀

▶

Back

Close

Full Screen / Esc

Printer-friendly Version

Interactive Discussion



Abstract

Lineshaped contrails were detected with the research aircraft Falcon during the CONCERT – CONtrail and Cirrus ExpeRiment – campaign in October/November 2008. Thereby the Falcon was equipped with a set of instruments to measure particle properties such as the particle size distribution, shape, extinction, chemical composition as well as trace gas concentrations of sulfur dioxide (SO₂), reactive nitrogen and halogen species (NO, NO_y, HNO₃, HONO, HCl), ozone (O₃) and carbon monoxide (CO). During 12 mission flights over Western Europe numerous contrails and cirrus clouds were probed at altitudes between 8.5 and 11.6 km and temperatures above 213 K. 22 contrails from 11 different aircraft were observed near and below ice saturation. The observed NO mixing ratios, ice crystal and soot number densities are compared to a process based contrail model. Further we investigate in detail the contrail from a CRJ-2 aircraft detected on 19 November 2008 in 10.1 km altitude. The contrail with an age of 1 to 2 min had average ice crystal concentrations of 128 cm⁻³ in the size range 0.4 < d < 17.7 μm. It was detected in ice subsaturated air at a mean ice saturation ratio of 0.87. The observation of particles with diameters larger than 100 μm in the contrail suggests that natural cirrus particles were entrained in the contrail. We further investigate oxidation reactions in the CRJ-2 engine and the contrail. The observed average HONO/NO (HONO/NO_y) ratios of 0.037 (0.024) are in the range of previous measurements in the gaseous exhaust. With HONO/NO ratio we can derive a lower limit of the conversion efficiency (ϵ_S) of fuel sulfur into H₂SO₄ of 2.9%. In addition to individual contrails and aircraft plumes, regional stratospheric NO enhancements were detected in the lowest stratosphere. Simulations show that aviation NO emissions could have contributed by more than 40% to the observed NO levels. Besides contrails, also cirrus clouds and a volcanic aerosol layer were measured during the CONCERT campaign. The observations serve to investigate the chemical processing of trace gases on contrails and help to better quantify the climate impact from contrails.

In situ observations of young contrails

C. Voigt et al.

Title Page

Abstract

Introduction

Conclusions

References

Tables

Figures

◀

▶

◀

▶

Back

Close

Full Screen / Esc

Printer-friendly Version

Interactive Discussion



1 Introduction

Aircraft induced cloudiness potentially has the largest aviation impact on climate (Lee et al., 2009). Yet the magnitude of its contribution to the anthropogenic radiative forcing remains highly uncertain (Penner et al., 1999; Lee et al., 2009). Aircraft induced cloudiness plays a role for the climate by interaction with solar and terrestrial radiation. Absorption and scattering of terrestrial infrared radiation by contrails induces a warming of the planetary surface. Scattering of incoming sunlight back into space increases the planetary albedo and leads to a cooling. In sum, aviation induced cloudiness contributes to the total anthropogenic radiative forcing and leads to a warming at the tropopause (Minnis et al., 1999).

Contrails form when the relative humidity in the young exhaust increases due to entrainment of the hot and humid exhaust with the colder and less humid ambient air (Schumann, 1996; Kärcher, 1996). When saturation with respect to water is reached, water condenses on soot and sulfate aerosol and forms liquid droplets. Thereby the aerosol originates from the combustion process or was entrained in the exhaust with the ambient air (Kärcher and Yu, 2009). When the exhaust further cools down through mixing with ambient air, ice saturation may be reached and ice nucleates in the liquid droplets (Kärcher and Yu, 2009) preferentially at ambient temperatures below 243 K (Schumann, 1996). Hence contrail formation and properties of young contrails may depend on the combustion process and on properties of the contrail-forming aircraft (Schumann, 1996; Sussmann and Gierens, 1999; Schumann et al., 2000). Further, model simulations suggest a dependence of contrail properties in the early vortex and in later contrail phases on ambient meteorology (Unterstrasser et al., 2008; Lewellen and Lewellen, 2001). When the ambient air remains supersaturated with respect to ice, the contrail ice crystals can grow by condensation of entrained water vapor and aggregation of aerosol (Schröder et al., 2000). Contrail dimensions and contrail coverage increase in ice supersaturated air due to mixing with ambient air, particle sedimentation and contrail spreading in an atmospheric environment with wind shear (Freudenthaler

In situ observations of young contrails

C. Voigt et al.

Title Page

Abstract

Introduction

Conclusions

References

Tables

Figures

◀

▶

◀

▶

Back

Close

Full Screen / Esc

Printer-friendly Version

Interactive Discussion



et al., 1995).

So far, few studies investigate microphysical properties of young contrails. Mean effective radii of contrail ice crystals derived from in situ data show values below 1 μm initially (Heymsfield et al., 1998), increasing due to condensation to values of up to 5 μm at 30 min contrail age (Schröder et al., 2000). Initial ice crystal concentrations larger than 1000 cm^{-3} have been detected in a few seconds old contrails (Heymsfield et al., 1998) decreasing by dilution within the first minutes to concentrations of less than 100 cm^{-3} (Fevbre et al., 2009). In persistent contrails with ages of 5 min to hours ice crystal concentrations of less than 20 cm^{-3} have been observed (Schäuble et al., 2009). Lidar measurements report contrail widths of 1–3 km for less than 30 min old contrails (Freudenthaler et al., 1995).

Little is known on chemical contrail properties and the uptake of HNO_3 in contrails. Gaseous HNO_3 has been detected in aircraft exhaust at cruise (Arnold et al., 1992; Tremmel et al., 1998). High levels of HNO_3 are expected in the young aircraft exhaust, which can be rapidly taken up by aircraft aerosol and contrails (Kärcher, 1996). At temperatures below 205 K, the gas phase HNO_3 is significantly reduced due to uptake in contrail ice crystals as detected for the contrail of a WB-57 at 14 km altitude (Popp et al., 2004). Nitric acid in the ice crystals at these temperatures might be present in the form of NAT (Gao et al., 2004; Voigt et al., 2008). Schäuble et al. (2009) show first quantitative measurements of the HNO_3 content in contrails. They report enhanced ice phase HNO_3 fractions in persistent contrails compared to natural cirrus clouds (Voigt et al., 2006; Kärcher and Voigt, 2006; Krämer et al., 2008). When the age of the contrail is known, the contrail ice crystals can serve as atmospheric laboratory for the study of the temporal evolution of trace gas uptake in ice crystals (Schäuble et al., 2009; Kärcher et al., 2009b).

Given the sparsity of in situ measurements of young contrails, measurements of chemical and optical contrail properties are of importance to better quantify their chemical and radiative impact on the atmosphere. Hence we report here on a new set of contrail observations. The measurements have been performed above Central Europe

**In situ observations
of young contrails**

C. Voigt et al.

Title Page

Abstract

Introduction

Conclusions

References

Tables

Figures

◀

▶

◀

▶

Back

Close

Full Screen / Esc

Printer-friendly Version

Interactive Discussion



**In situ observations
of young contrails**

C. Voigt et al.

[Title Page](#)[Abstract](#)[Introduction](#)[Conclusions](#)[References](#)[Tables](#)[Figures](#)[◀](#)[▶](#)[◀](#)[▶](#)[Back](#)[Close](#)[Full Screen / Esc](#)[Printer-friendly Version](#)[Interactive Discussion](#)

and Germany with the DLR research aircraft Falcon during the CONCERT (CONtrail and Cirrus ExperRiment) campaign from 22 October to 20 November 2008. Within the first two weeks of the campaign (CONCERT-CHEMISTRY) we focussed on measurements of the heterogeneous chemistry on aerosol, cirrus and contrails, while the detection of microphysical and optical contrail properties was within the scope of the second part of the campaign (CONCERT-2-CONTRAIL). During the CONCERT campaign, cirrus clouds were encountered during 10 mission and 2 instrument test flights for almost 2 h. 22 contrails from 11 different aircraft were sampled in total for 1.7 h at temperatures from 213 to 229 K (27 and 28 October and 2, 17, 19 and 20 November 2008). Here we use the contrail observations for model validation. Further, we investigate in detail the microphysical properties from a CRJ-2 contrail and analyze the chemical processing of SO₂ and NO in the engine and the young contrail. Further, large scale aircraft NO emissions were predicted from global model simulations and measured during two mission flights on 31 October 2008.

In addition, a sulfate aerosol layer was detected in the lowermost stratosphere at altitudes between 7 and 11.6 km (28 and 31 October 2008). The layer most likely originated from the eruption of the Aleutian volcano Mt. Kasatochi on 7/8 August 2008, the largest volcanic eruption since Mt. Pinatubo in 1991 injecting 1.4 Mt SO₂ into the high latitude stratosphere. We discuss the chemical processing of sulfur and halogens species in the aged volcanic plume and derive the e-folding lifetime of SO₂ in the northern latitude lowest stratosphere.

2 Aircraft instrumentation

During the CONCERT campaign the DLR research aircraft Falcon was equipped with a set of instruments to detect trace gases as well as microphysical and radiative particle properties with the aim to investigate the chemical and the radiative impact of contrails, cirrus cloud and aerosol particles on the atmospheric composition and climate.

2.1 The Ion Trap Chemical Ionization Mass Spectrometer (ITCIMS)

An ion trap chemical ionization mass spectrometer (ITCIMS) (Fiedler et al., 2005; Speidel et al., 2007; Fiedler et al., 2009) was for the first time operated with SF₅⁻ reagent ions for the detection of HCl, HNO₃, SO₂ and HONO in the UTLS. A detailed description of the instrument is given in Jurkat et al. (2010). An in-flight calibration was performed by the use of a nitric acid permeation standard in a newly designed permeation oven embedded in a latent heat reservoir. In the flow reactor SF₅⁻ reacts with the four trace gases via a fluoride transfer, here exemplarily shown for reactions with SO₂ and with HONO:



The water clusters are removed through collision with helium injected into the ion trap. Mass spectra from 15 to 170 atomic mass units (amu) with a resolution of 0.3 amu were sampled during a trapping time of 200 ms and averaged over five spectra resulting in an overall time resolution of 1.6 s. This allowed for the fast and sensitive detection of SO₂ and HONO in young exhaust plumes of commercial airliners and for measurements of SO₂, HCl and HNO₃ in an aged stratospheric plume of volcanic origin. Detection limits for HONO and SO₂ for 1.6 s time resolution were 72 and 67 pmol/mol (pptv). Detection limits for HCl and HNO₃ were 22 and 36 pmol/mol respectively with a running mean over 20 spectra (approx. 32 s). HCl, SO₂ and HONO were calibrated in the laboratory. The HONO calibration of the ion trap mass spectrometer was carried out with a LOPAP instrument (Heland et al., 2001) proving the pseudo first order kinetic reaction (Eq. 2) given above. The calibration factor accounting for the rate coefficient, the ion molecule reaction time, the dilution and possible wall effects for SO₂ and HONO were 20 and 10 nmol/mol (ppbv) with an instrumental error of ±25% and 40%, respectively.

[Title Page](#)[Abstract](#)[Introduction](#)[Conclusions](#)[References](#)[Tables](#)[Figures](#)[◀](#)[▶](#)[◀](#)[▶](#)[Back](#)[Close](#)[Full Screen / Esc](#)[Printer-friendly Version](#)[Interactive Discussion](#)

2.2 The NO_y instrument

The NO_y instrument is described in detail in Ziereis et al. (2004) and Voigt et al. (2005). During the first two weeks of the campaign (CONCERT-CHEMISTRY), it was configured to detect gas phase reactive nitrogen NO_{y,g} (=NO + NO₂ + HONO + HNO₃ + 2N₂O₅ + PAN + ...). with a backward facing inlet and total NO_{y,t} (=NO_{y,g} + NO_{y,part}) with a forward facing inlet. During the second part of the campaign (CONCERT-2-CONTRAIL) it was configured to detect gaseous NO_{y,g} and nitric oxide (NO) with two backward facing inlets.

In brief, the detection principle of the NO_y instrument is based on the evaporation of particles in the forward facing inlet, the reduction of gaseous NO_y to NO with CO in a heated gold converter and the detection of the chemiluminescence reaction of NO with ozone. Thereby the converter unit is bypassed for the detection of NO. The NO_y instrument has a detection limit of 1 and 5 pmol/mol for NO and NO_y, respectively, and an accuracy of ±8%.

By subtracting the gas phase NO_{y,g} from the total NO_{y,t} we can calculate the enhanced particulate NO_{y,part} mixing ratio (Voigt et al., 2007). NO_{y,part} has to be divided by the pressure and size dependent particle enhancement factor to estimate the NO_{y,part} content in cloud particles. The method to evaluate particulate NO_{y,part} is described by Voigt et al. (2005).

2.3 The Fast In Situ Hygrometer FISH

Water vapor was measured with the closed path Fast In situ Stratospheric Hygrometer (FISH) (Zöger et al., 1999; Schiller et al., 2008) using the Lyman- α photofragment fluorescence technique. H₂O mixing ratios between 0.5 and 1000 ppmv can be detected with FISH with a time resolution of 1 s and an overall accuracy of 6% or at least 0.3 ppmv. FISH is calibrated regularly before, during and after the field campaign using calibration bench including a frost point hygrometer (MBW DP30) as reference. During CONCERT, air is probed by a backward facing inlet tube, i.e. FISH measured gas

Title Page

Abstract

Introduction

Conclusions

References

Tables

Figures

◀

▶

◀

▶

Back

Close

Full Screen / Esc

Printer-friendly Version

Interactive Discussion



phase water (H_2O_g). Including the uncertainty of 0.5 K for the temperature measurements, the relative humidity (RH) can be determined with an uncertainty of $\pm 15\%$.

2.4 The frost point hygrometer

In addition water vapor has been detected with the cryogenic frost point hygrometer CR-2 (Buck Research Instruments, LLC) on the Falcon. The instrument measures the temperature of a mirror carrying a thin frost layer that is maintained in equilibrium with the ambient water vapor. The bulk reflectivity of the mirror is measured with an optical detector. It initializes a control circuit to regulate the mirror temperature such that the bulk reflectivity and hence the condensate layer remain constant or in thermal equilibrium with the air passing over the mirror. The mirror temperature is then equal to the ambient frost point temperature and the water vapor mixing ratio and relative humidity can be calculated from this measurement using the inverse Clausius-Clapeyron equation.

The uncertainty of the water vapor mixing ratio is between $\pm 3\%$ and $\pm 5\%$ for water vapor mixing ratios between $340 \mu\text{mol}/\text{mol}$ and $40 \mu\text{mol}/\text{mol}$. This uncertainty does not include time-dependent oscillations of the mirror temperature induced by the control circuit after strong humidity changes. Therefore, depending on the water vapor concentration changes, the response time of the frost point hygrometer is in the order of one minute to few seconds. The frost point hygrometer has been compared to a high accuracy laboratory frost point hygrometer during and after the campaign. It has been operated for the first time on the Falcon during the CONCERT mission.

2.5 The Aerosol Mass Spectrometer AMS

The chemical composition and size distribution of submicron aerosol particles were determined by an Aerodyne Compact Time-of-Flight Mass Spectrometer (C-ToF-AMS). The instrument samples aerosol through an aerodynamic lens system which focuses the particle beam onto a vaporizer operated at 600°C . Before reaching the vaporizer,

In situ observations of young contrails

C. Voigt et al.

Title Page

Abstract

Introduction

Conclusions

References

Tables

Figures

◀

▶

◀

▶

Back

Close

Full Screen / Esc

Printer-friendly Version

Interactive Discussion



the particles pass through a time-of-flight region in a vacuum chamber that allows for particle size determination. The vapor is ionized by 70 eV electrons, and the generated ions are analyzed in a time-of-flight mass spectrometer. For a detailed description of the C-ToF-AMS see Canagaratna et al. (2007); Drewnick et al. (2005). During CONCERT-CHEMISTRY particulate sulfate, ammonium, nitrate, chloride and carbonaceous matter were determined for STP conditions with a time resolution of 10 s. The respective detection limits were 0.02, 0.13, 0.02, 0.03, and 0.11 $\mu\text{g m}^{-3}$ (STP) on campaign average. To compensate for the decreasing mass flow into the instrument with altitude a pressure controlled inlet (PCI) was installed in front of the standard AMS inlet system, also guaranteeing isokinetic sampling from the aircraft's aerosol inlet (for a more thorough description of the inlet system and the characterization of the PCI see Schmale et al. (2010). This Falcon-specific set-up allowed for sampling of particles in the size range between 84 and 735 nm vacuum aerodynamic diameter.

2.6 The Forward Scattering Spectrometer Probe FSSP300

Particle size distribution and number density were detected with a forward scattering spectrometer probe (Schröder et al., 2000). The FSSP300 detects light scattered by particles in the diameter range 0.45–17.7 μm . The particles were grouped into size channels according to T-matrix calculations by Borrmann et al. (2000) assuming aspherical particles with an aspect ratio of 1:2 composed of pure ice with a refractive index of 1.31. Adjustments of the mean channel size were made to account for instrumental manufacturing differences. Further FSSP channels 8+9, 10+11, 12+13+14+15, 16+17, 18+19, 20+21+22+23+24, 25+26, 29+30 were grouped to increase the counting statistics particularly in channels with a small channel widths. This data evaluation method proved to achieve best agreement between the FSSP and the polar nephelometer data.

In situ observations of young contrails

C. Voigt et al.

Title Page

Abstract

Introduction

Conclusions

References

Tables

Figures

◀

▶

◀

▶

Back

Close

Full Screen / Esc

Printer-friendly Version

Interactive Discussion



2.7 The 2DC probe, the Polar Nephelometer (PN) and the Cloud Particle Imager (CPI)

The particle size distribution of large particles (20 μm to 1 mm) was measured with a 2DC probe, the particle shape (2.3 μm pixel size) with a cloud particle imager (CPI) and the scattering phase function of cloud particles (3 μm to 1 mm) with a Polar Nephelometer (PN). The method of data processing, the reliability of the instruments and the uncertainties of the derived microphysical and optical parameters have been described in detail by Gayet et al. (2009).

The CPI records very high resolution (2.3 μm) digital images of cloud particles as they pass through the sample tube of the instrument. It casts an image of the particle on a solid-state CCD camera by freezing the motion of the particle using a 25 ns pulsed, high-power laser diode. Upstream lasers precisely define the depth-of-field so that at least one particle in the image is almost always in the focus. This eliminates out-of-focus sizing errors that have plagued the conventional 2-D imaging probes. The method of data processing leads to derive the particle size distribution and calculates the usual microphysical parameters: ice particle concentration, extinction coefficient, mean particle size, and ice water content. The classification of the shape of the ice particles can also be derived.

The Polar Nephelometer (PN) is designed to measure the optical and microphysical parameters of clouds containing either water droplets or ice crystals or a mixture of these particles over a size range from a few micrometers to about 800 microns diameter. The probe measures the scattering phase function of an ensemble of cloud particles which intersect a collimated laser beam near the focal point of a paraboloidal mirror. The light scattered from polar angles from $\pm 3.49^\circ$ to $\pm 169^\circ$ is reflected onto a circular array of 54 photodiodes. The signal processing electronics and computer storage can provide one measurement of the scattering phase function every 10 ms. The optical properties (extinction coefficient, asymmetry factor, backscattering coefficient) are derived from the measured scattering phase functions. The particle size spectra

In situ observations of young contrails

C. Voigt et al.

Title Page

Abstract

Introduction

Conclusions

References

Tables

Figures

◀

▶

◀

▶

Back

Close

Full Screen / Esc

Printer-friendly Version

Interactive Discussion



and subsequent derived quantities such bulk and size parameters are retrieved using an inversion technique. The particle phase discrimination (water droplet/ice particles) can be derived from the shape of the scattering phase function.

2.8 The Cloud Imaging Probe CIP

5 During the last flight the 2DC has been exchanged with a Cloud Imaging Probe (CIP), which is a new version of the 2DC, for instrument comparison with the CPI. The CIP measures the size and shape of particles passing through its collimated laser beam, from 25 μm to 1600 μm with a resolution of 25 μm . It is capable to detect particle concentrations up to 100 cm^{-3} at airspeeds up to 200 m/s. It uses a fast 64-element
10 photodiode array to generate 2-dimensional images of the particles. Included in this instrument package are temperature, pressure and relative humidity sensors. As for the FSSP, the uncertainty in the CIP particle number concentration is mainly determined by the uncertainty in the sample volume. At low particle concentrations also counting statistics have to be taken into account. The uncertainty in the sample volume is estimated to be 20%. Important for the calculation of the particle size distribution and
15 volume concentration is the uncertainty in the particle size. This uncertainty decreases considerably with particle size and is $\pm 25 \mu\text{m}$ for particles $> 50 \mu\text{m}$ in diameter (De Reus et al., 2009).

2.9 The Spectral Modular Airborne Radiation measurement sysTem (SMART)-Albedometer

20 Spectral upwelling radiances and irradiances were measured with the Spectral Modular Airborne Radiation measurement sysTem (SMART)-Albedometer (Wendisch et al., 2001). During the CONCERT campaign, an optical inlet with a viewing angle of 1.5° designed to measure radiances as well as an irradiance optical inlet (half-dome shape)
25 were each connected to two plain-grated spectrometers, respectively. The optical inlets were placed in the back part of the fuselage of the aircraft. The spectrometers operate

In situ observations of young contrails

C. Voigt et al.

Title Page

Abstract

Introduction

Conclusions

References

Tables

Figures

◀

▶

◀

▶

Back

Close

Full Screen / Esc

Printer-friendly Version

Interactive Discussion



in the wavelength ranges 350 to 1050 nm and 900 to 2200 nm with spectral resolutions (Full Width at Half Maximum, FWHM) of 2 to 3 nm and 9 to 16 nm, respectively. The temporal resolution of the measurements is in the order of 0.5 to 3 s, corresponding to a spatial resolution of 100 to 600 m at an aircraft velocity of 200 m/s.

3 Flight planning and meteorological forecasts

Research flight planning was based on deterministic meteorological forecasts from the European Centre for Medium-Range Weather Forecasts (ECMWF) and on chemical forecasts computed by the MATCH-MPIC model (Lawrence et al., 2003). In addition to the forecast quantities provided by ECMWF, we derived several campaign-specific forecast quantities, for instance, the Schmidt-Appleman criterion (Schumann, 1996) to predict regions with a high likelihood of contrail occurrence. Furthermore, the trajectory code LAGRANTO (Wernli et al., 1997) was run on-demand on the ECMWF predicted wind fields in order to estimate how contrails in the flight target regions would be advected.

ECMWF forecasts were visualized with the Metview system (Bonifacio, 1999) and made available to the campaign scientists through a web-based user interface. For fast on-demand LAGRANTO computations, a Python-based user interface was developed. With the information given by the forecast system, we were able to identify target regions with atmospheric conditions well suited to fulfil the mission objectives. Figure 1 shows a plot of the 36 h forecast of the Schmidt-Appleman criterion combined with regions of high relative humidity, valid on 19 November 2008, 12:00 UTC, at 250 hPa. The predictions indicated good conditions for contrail occurrence over Germany and the North Sea. The day was subsequently chosen for targeted contrail observations.

In situ observations of young contrails

C. Voigt et al.

Title Page

Abstract

Introduction

Conclusions

References

Tables

Figures



Back

Close

Full Screen / Esc

Printer-friendly Version

Interactive Discussion



4 Flight survey

During the CONCERT campaign, the Falcon performed 12 mission flights on 27, 28, 29 and 31 October and on 2, 7, 17, 19 and 20 November 2008 including 3 return flights on 31 October and on 17 and 19 November. The flight paths from all flights are shown in Fig. 2. Extensive contrail measurements were performed on 2, 17, 19 and 20 November and contrails were also observed on 28 and 29 October, but without FSSP data. The flights on 27 October and on 7 and 20 November also concentrated on the detection of cirrus clouds. The 31 October return flight from Oberpfaffenhofen to Shannon had the aim to detect regional aircraft emissions from the Northern Atlantic flight corridor. Sampling a stratospheric intrusion was the main goal for the flights on 28 and 31 October.

5 Detection of young contrails

Microphysical and optical properties of 22 young contrails were detected by the instruments aboard the Falcon on 8 mission flights. Contrails from 11 different aircraft types were detected, including an A380, several A340s and B767s and B737s, an A319, a CRJ-2 and a Fokker20. The contrails were probed at altitudes between 8.5 to 11.6 km and at temperatures between 213 and 229 K (Fig. 3). Contrails were identified from a simultaneous increase in the extinction $> 0 \text{ km}^{-1}$ and the NO mixing ratio $> 0.2 \text{ nmol/mol}$, latter representing the upper limit for the upper tropospheric NO levels. Further the threshold temperature $T < 240 \text{ K}$ was used to exclude lower tropospheric cloud observations. In total 1.7 h of contrail measurements were achieved. The contrails were sampled at RHI between 122 and 55%, with 80% of the observations concentrating at 105 to 75% RHI. Including the error in the temperature measurements, the RHI has an accuracy of $\pm 15\%$. Hence contrail ice crystals were detected in air that was frequently sub-saturated with respect to ice.

Contrails were mainly probed in the top region or above visible cirrus clouds, as

Title Page

Abstract

Introduction

Conclusions

References

Tables

Figures

◀

▶

◀

▶

Back

Close

Full Screen / Esc

Printer-friendly Version

Interactive Discussion



5 this sampling strategy was found to be very effective. This might also explain why the maximum in the RHI distribution is found below 100% (see Fig. 3). The contrail sampling strategy was the following: Predictions of the IWC from the ECMWF were used to send the aircraft into the top of a cirrus cloud. The Falcon further ascended above the cloud till contrails were observed by the pilots. The contrail formation altitude was communicated to German Air Traffic Control (DFS), and commercial airliners crossing that region were asked to change their flight altitude to contrail formation altitudes. Thereafter the Falcon was directed behind the airliners and contrails were probed at 10 to 86 nautical miles distance corresponding to contrail ages of 55 to 570 s. During the contrail samplings, the pilots of the commercial aircraft communicated their distance to the Falcon as well as aircraft parameters such as velocity, weight and fuel flow. These parameters were then used to derive emission indices for NO_x at flight altitude (Schulte et al., 1997; Döpelheuer and Lecht, 1999).

5.1 Survey of two contrail flights on 19 November 2008

15 On 19 November 2008, extensive contrail measurements were performed with the Falcon. We detected 10 contrails above Germany during a return flight from Oberpfaffenhofen to Hamburg and back. During the first flight shown in Fig. 4, we frequently chased an A319, which was a charter aircraft flying specifically for the contrail measurements. The exhaust of the A319 without contrail was detected in the first encounter, thereafter contrails from the A319 were probed four times with the longest contrail encounter of 20 13 min. In addition, the contrail from an A340 was sampled twice. During the return flight, we chased four commercial aircraft and detected the contrails of a B767, a CRJ-2, an A380 and an A320 over Germany as shown in Fig. 5.

25 Contrail encounters are marked by fast simultaneous increases in the NO mixing ratio, the particle number density detected with the FSSP and the extinction detected with the PN. Again, we attribute contrails to measurements with the extinction $> 0 \text{ km}^{-1}$ and the NO mixing ratio $> 0.2 \text{ nmol/mol}$ and FSSP particle concentrations $> 10 \text{ cm}^{-3}$. The contrails were filmed by the camera in the cockpit of the Falcon.

In situ observations of young contrails

C. Voigt et al.

Title Page

Abstract

Introduction

Conclusions

References

Tables

Figures

◀

▶

◀

▶

Back

Close

Full Screen / Esc

Printer-friendly Version

Interactive Discussion



**In situ observations
of young contrails**

C. Voigt et al.

Title Page

Abstract

Introduction

Conclusions

References

Tables

Figures

◀

▶

◀

▶

Back

Close

Full Screen / Esc

Printer-friendly Version

Interactive Discussion



Highest NO mixing ratios and extinctions were detected in the contrail of the A380. The contrail was observed for 756 s. NO values up to 58 nmol/mol were observed and the extinction of particles with $d > 3 \mu\text{m}$ increased to 5.4 km^{-1} in the A380 contrail. Enhanced particle concentrations ($0.4 < d < 17.7 \mu\text{m}$) up to 537 cm^{-3} were detected. Average values in the A380 contrail were lower with a particle concentration of 179 cm^{-3} , NO mixing ratio of 6 nmol/mol and extinction of 1.6 km^{-1} .

The age of the contrails has been calculated based on the positions of the Falcon and the contrail producing aircraft taking into account the drift of the contrail at the measured wind speed. The ages of the detected contrails were between one and three minutes for the A319, the A340, the B767 and the CRJ-2. The A380 was detected for 16 min at ages of 1 to 5 min. Having left the contrail of the A380, the contrail of an A320 was sampled at ages of 8 to 10 min, representing the oldest contrail sampling during the CONCERT campaign. All contrails are expected to be line shaped as they are less than 10 min old. Hence the contrail measurements were performed in the vortex and the early dispersion regime.

6 Contrail modeling

A new “Contrail Cirrus Prediction Tool” (CoCiP) has been developed to simulate contrail cirrus resulting from a single flight as well as from a fleet of cruising aircraft, flight by flight, regionally or globally (Schumann, 2009). The method predicts contrail cirrus for given aircraft, traffic and weather prediction data. The method describes the life cycle of individual contrails using a Lagrangian Gaussian plume model, following early concepts (Schumann and Konopka, 1994; Konopka, 1995; Schumann et al., 1995). The turbulent mixing of the plume is mainly controlled by shear but also controlled by turbulent diffusivities; these parameters were selected such that the computed dilution factor (i.e. the mass of the plume per mass of fuel burnt) fits available measurements (Schumann et al., 1998) and LES results (Dürbeck and Gerz, 1996). Contrails are initiated when the Schmidt-Appleman criterion is satisfied (Schumann, 1996). The evolution of

**In situ observations
of young contrails**

C. Voigt et al.

[Title Page](#)[Abstract](#)[Introduction](#)[Conclusions](#)[References](#)[Tables](#)[Figures](#)[◀](#)[▶](#)[◀](#)[▶](#)[Back](#)[Close](#)[Full Screen / Esc](#)[Printer-friendly Version](#)[Interactive Discussion](#)

the individual contrails is computed using wind, temperature, humidity, and ice water content from numerical weather prediction (NWP) output. In our case we use the operational forecast data of the Integrated Forecast System of the European Centre for Medium Range Weather Forecast. This model computes the humidity, allowing for ice supersaturation in air masses without and with cirrus clouds, in fair agreement with observations (Tompkins et al., 2007). The plume trajectory follows horizontal and vertical winds using established methods (Stohl et al., 2001). The ice phase is modelled as a function of bulk contrail ice properties (ice mass and ice particle number). It is assumed that ice particles form on emitted soot particles. The ice water content is computed as a function of mixing and ambient humidity. The model assumes ice saturation inside the contrail. Contrails in subsaturated air masses evaporate at time scales depending on the emitted mass of water vapor, the degree of subsaturation and plume dilution. In supersaturated air masses, the contrail ice water content grows by uptake of humidity mixed into the plume from ambient air. The final life time of the contrails in the model is controlled by ice particle loss processes (turbulent mixing, aggregation, sedimentation, radiative heating). These aspects will be described elsewhere and are not important for the present study with young contrails. The climate impact of the contrails (radiative forcing and radiative energy gain per flight distance with contrail) is computed as a function of the contrail properties (width, length, life time, optical depth, temperature, effective radius, optical depth of ambient cirrus above the contrail) using radiative fluxes without contrails from NWP output (Schumann, 2009).

The contrail properties are strongly dependent on the ambient meteorological field (in particular humidity, shear, stratification, and upward motion). In addition the computed contrail properties are aircraft depending (Schumann, 1996). The fuel properties and the propulsion efficiency of the aircraft influence the threshold temperature of contrail formation (Busen and Schumann, 1995). The amount of water vapor emitted in the early contrail contributes to the initial ice water content and hence the life time of the contrail in unsaturated ambient air. The number of soot particles emitted controls the number of ice particles forming in the young contrail (Kärcher and Yu, 2009).

Besides fuel consumption, the emission indices (EI) control the computed plume concentrations. The emission index for NO_x was determined as in Döpelheuer and Lecht (1999) based on aircraft and engine type and the fuel consumption rates reported by the aircraft pilots. The mass, speed and span width of the individual aircraft determine the downward sinking of the wake vortex (Holzäpfel, 2006). The shear driven plume dispersion is strongly enhanced for large wake vortex sinking depths (Schumann et al., 1995). The actual air traffic data (radar observed aircraft type and aircraft positions versus time) were provided for the CONCERT days by the Deutsche Flugsicherung (DFS). The position of the Falcon, measured onboard was found to be in close agreement (50 m laterally, 10 m vertically) with the DFS observations.

6.1 Validation of CoCiP model results with CONCERT observations of young contrails

From the position of the Falcon as a function of time, and the ECMWF forecast wind field (wind speed of order 40 m/s), the model computes the age of the exhaust plume at the time of measurement. The data were accurate enough to decide when the Falcon was in or near the exhaust of aircraft for young plumes (a few minutes) to an age dependent accuracy of order 300 m horizontally, and 20 m vertically. Figure 6 shows the plume ages (between 60 and 600 s) for the two Falcon flights of 19 November 2008. Also plotted is the fuel consumption of the aircraft, which varies by a factor of 20 between the various aircraft. Form a comparison of the computed and measured times of entering the exhaust plume we could see that the model correctly predicts the sinking of the initial wake vortices, up to 270 m for the heaviest aircraft, to within about 20 m vertical accuracy. Figure 7 shows the NO_x mixing ratio versus Falcon flight time. Both 1-s data and 10-s running averages of the measured data are plotted. The latter are commensurable with the model results which do not resolve the turbulent details of the aircraft wake. In the model, the simulated Falcon track does not always lead through the rather narrow (order of 100 m) exhaust plume. Hence the model tends to underestimate the maximum measured exhaust concentrations. However, the model can also

In situ observations of young contrails

C. Voigt et al.

[Title Page](#)[Abstract](#)[Introduction](#)[Conclusions](#)[References](#)[Tables](#)[Figures](#)[◀](#)[▶](#)[◀](#)[▶](#)[Back](#)[Close](#)[Full Screen / Esc](#)[Printer-friendly Version](#)[Interactive Discussion](#)

be applied to compute the plume properties under the assumption that the Falcon at the time of measurement would be flying exactly in the center of the Gaussian plume. In this way, the model provides the maximum exhaust values that are consistent with the Gaussian plume. The NO_x data reach up to 50 nmol/mol, i.e., far above the background concentrations. Maximum concentrations were measured in the plume of the biggest aircraft (A380). The maximum concentrations decrease with plume age because of dilution. Figure 7 shows that the model provides NO_x mixing ratios that are within the scatter of the measured data. The model gives different NO_x levels in the various plumes which differ because of different plume ages, dilution, fuel consumption and emission indices. For comparable plume ages, the NO_x concentration is larger for heavier aircraft, mostly with higher emission indices. The results indicate that the model parameters were suitably selected to correctly simulate the dilution in the sheared and turbulent ambient atmosphere. It should be noted that this agreement was obtained after the emission indices had been adjusted for the various aircraft/engine types. The results indicate quite large NO_x emission indices in some cases (up to 27 g/kg). Figure 7 shows similar results for the ice crystal number concentration in the contrail. The model results and the measurements (for ice particles larger than 1 μm) agree within the scatter of the data. The concentrations reach as high as 100 cm^{-3} in the contrails. During the first flight the model tends to overestimate the ice particle concentrations and predicts very small ice water content because of the low ambient humidity. The agreement with observations is better during the second flight at higher ambient humidity. The computed ice particle concentration is linearly dependent on the number of soot particles emitted with the exhaust. Hence, this is also a check for the soot number emission indices used ($2.4\text{--}3.4 \times 10^{15} \text{ kg}^{-1}$). The absolute level of the model results is sensitive to the plume dilution and the loss of ice particles in the adiabatically sinking and thus heating wake core contrail (Sussmann and Gierens, 1999; Unterstrasser and Gierens, 2010; Lewellen and Lewellen, 2001). Again the agreement is such that it supports the basic validity of the model.

**In situ observations
of young contrails**

C. Voigt et al.

Title Page

Abstract

Introduction

Conclusions

References

Tables

Figures

◀

▶

◀

▶

Back

Close

Full Screen / Esc

Printer-friendly Version

Interactive Discussion



**In situ observations
of young contrails**

C. Voigt et al.

Title Page

Abstract

Introduction

Conclusions

References

Tables

Figures

◀

▶

◀

▶

Back

Close

Full Screen / Esc

Printer-friendly Version

Interactive Discussion



CoCiP seems to compute realistic ice particle concentrations. There were no indications of additional ice formation beyond soot induced ice particles. In particular, there are not indications for large contributions from volatile material contributing to ice nucleation for these cases with temperatures of 210 to 222 K. Hence, it seems that the rather complex issue of ice formation in fresh contrails can be explained at accuracy comparable with measurements with a Gaussian plume model and with bulk ice physics and nucleation controlled by the soot particles in the contrail.

Further model tests are underway to explain observed aviation induced cirrus cover diurnal changes over the North Atlantic. The model is computationally efficient enough to be used in forecast mode for operational route optimization with respect to minimum climate impact. The model can be used to evaluate the radiative forcing induced by contrail cirrus formation globally.

7 Detailed investigation of the contrail from a CRJ-2 aircraft

Below we discuss in detail the contrail sampling from the CRJ-2 on 19 November 2008. The aircraft was chased between 11:40:23 and 11:45:06 UT above Germany (Fig. 8). The contrail was detected for almost 4.5 min at an altitude of 10.02 to 10.11 km and at temperatures near 221.4 ± 0.1 K. Elevated extinction up to 3.3 km^{-1} , particle number concentrations up to 406 cm^{-3} and NO mixing ratios up to 6 nmol/mol were measured. Average values in this contrail are 0.8 km^{-1} in the extinction, 126 cm^{-3} in the particle concentration and 1.7 nmol/mol in the NO mixing ratio. Further peak SO_2 and HONO mixing ratios of up to 0.69 and 0.26 nmol/mol were detected. In the contrail the RHI increased to values between 82 and 95% and was below these values direct before and after the encounter. The contrail was detected at an age of 61 to 122 s and hence was probed in the vortex regime.

The particle surface and volume distributions detected in the contrail is shown in Fig. 9. The particle size distribution has been derived from the FSSP and the 2DC measurements. The count rate in each channel of the particle probes has been averaged

over the total contrail sampling time. To assure that we were inside the contrail with the particle probes on both wings of the Falcon and to discriminate measurements at the edge of the contrails, only particle data at NO concentrations >0.2 nmol/mol were integrated.

Also shown is the particle size distribution of the surrounding cirrus field. The cirrus cloud has been detected after leaving the contrail from 11:45:06 UT for 5 min as indicated by background NO and SO₂ mixing ratios and elevated extinction and particle number density. The cirrus cloud has been observed at altitudes between 10.1 and 10.4 km and temperatures of 221 to 219 K. The cirrus particle size distribution (see Fig. 9) suggests that the contrail was embedded in a cirrus cloud and that the large cirrus crystals ($d > 100 \mu\text{m}$) might have been entrained in the contrail. While contributing only a minor fraction to the total contrail particle surface area, the large particles may have an effect on the total contrail particle volume.

In the contrail, the small particle mode with $d < 17.7 \mu\text{m}$ is clearly dominated by contrail ice crystals and is only slightly influenced by cirrus crystals. Figure 9 also shows that inlet effects from the FSSP do not significantly disturb the cirrus and contrail measurements.

The contrail particle size distribution for particles with $0.45 < d < 17.7 \mu\text{m}$ yields a mean ice crystal surface A of $1.81 \times 10^{-9} \mu\text{m}^2 \mu\text{m}^{-3}$ and a mean contrail ice volume V of $5.2 \times 10^{-10} \mu\text{m}^3 \mu\text{m}^{-3}$. Using the equation $r_{\text{eff}} = (3/4) V/A$ yields an effective radius r_{eff} of $2.6 \mu\text{m}$. The contrail particle size distribution broadly agrees with observations in a less than 3 min old contrail by Schröder et al. (2000).

7.1 Processing of NO and SO₂ in the engine and the plume/contrail from the CRJ-2 aircraft

Amongst gaseous aircraft emissions, SO₂ and NO_x are the most important precursors for condensable acids that influence particle formation and composition in the upper troposphere. The rate of conversion of fuel sulfur into H₂SO₄, e_S , has been subject to many investigations (Fahey et al., 1995; Curtius et al., 1998; Miake-Lye et al., 1998)

In situ observations of young contrails

C. Voigt et al.

[Title Page](#)[Abstract](#)[Introduction](#)[Conclusions](#)[References](#)[Tables](#)[Figures](#)[◀](#)[▶](#)[◀](#)[▶](#)[Back](#)[Close](#)[Full Screen / Esc](#)[Printer-friendly Version](#)[Interactive Discussion](#)

with recent estimates of ϵ_S ranging from 2 to 10%. Simultaneous measurements of HONO, NO and SO₂ in aircraft exhaust plumes under cruise conditions do not exist. HONO/NO ratios have been measured in flight (Arnold et al., 1992) and HONO/NO_x ratios on the ground (Wormhoudt et al., 2007; Wood et al., 2008) with an average of 2% for thrust settings between 30 and 100%.

As an example we discuss here the encounter of the CRJ-2 contrail with a CF34-3B engine detected on 19 November 2008 shown in Fig. 5. A good correlation of the NO mixing ratios detected with a chemiluminescence detector and the HONO and SO₂ mixing ratios measured with the ITCIMS instrument has been observed. Within the plume HONO mixing ratios range from 0.26 nmol/mol to values below the detection limit and SO₂ shows peak values of 0.69 nmol/mol with a background of 0.08 to 0.1 nmol/mol.

The HONO/NO ratio was calculated by integrating over all measurements in the contrail to account for the different time resolution of the two instruments. For this aircraft and plume ages of 62 to 122 s, HONO/NO (HONO/NO_y) ratios were 0.037 (0.024) with an instrumental error of $\pm 42\%$. The high HONO/NO value suggests that NO conversion to NO₂ has occurred within in the first minute after emission. Higher HONO/NO values are therefore expected in aging plumes compared to measurements at the engine exit (Wood et al., 2008).

In order to derive the conversion efficiency of fuel sulfur ϵ_S in the engine we compare the two formation pathways of HONO and HSO₃ (a precursor of H₂SO₄) in the turbine segment of the engine. A major part of the OH-induced conversion of the precursor gases SO₂ and NO takes place in the combustion chamber and the turbine segment of the engine (Kärcher et al., 1996; Somnitz et al., 2005). Here SO₂ reacts with OH via the Stockwell-Calvert-Mechanism to form H₂SO₄ and NO reacts directly with hydroxyl radicals to form HONO. Under the assumption that the ratio of the effective rate coefficients for the two reactions is near unity the sulfur conversion efficiency can be inferred.

**In situ observations
of young contrails**

C. Voigt et al.

[Title Page](#)[Abstract](#)[Introduction](#)[Conclusions](#)[References](#)[Tables](#)[Figures](#)[◀](#)[▶](#)[◀](#)[▶](#)[Back](#)[Close](#)[Full Screen / Esc](#)[Printer-friendly Version](#)[Interactive Discussion](#)

In the case of the CRJ-2 the fuel sulfur conversion efficiency yields a value of 2.9%. This fraction can be regarded as a lower limit because our method accounts specifically for the OH-induced conversion of SO₂. This lower limit is in good agreement with recent model simulations of the sulfur conversion efficiency (Starik et al., 2002), and compares well with former direct in-situ measurements of total sulfuric acid (Curtius et al., 2002) in aircraft exhaust plumes. The uncertainty of the method arises from the uncertainty of the effective rate coefficients for the reaction SO₂+OH and NO+OH. The advantage of this method to derive the sulfur conversion efficiency is that it is independent of dilution and the initial OH concentration and it benefits from reliable trace gas measurements.

8 Aircraft NO corridor effects in the lowermost stratosphere

Besides small scale plume processing also the detection of regional scale aircraft emissions were within the scope of the CONCERT campaign.

Therefore, the MATCH-MPIC model (Lawrence et al., 2003) was used for the prediction of regional aircraft NO emissions. The MATCH-MPIC model is a global, three-dimensional chemical transport model driven by meteorological analyses and forecasts from NCEP (National Centers for Environmental Prediction). During the CONCERT campaign, MATCH-MPIC was run semi-operationally in two configurations, one with, and the other without aircraft NO emissions. Aircraft emissions used for these simulations are described by Schmitt and Brunner (1997). Examination of the differences between the output from these two model configurations allowed the prediction of large-scale regions influenced by aircraft emissions. Figure 10 shows examples of the background and the aircraft NO predictions for 31 October 2008, 12:00 UTC, at 250 hPa including the flight path of the Falcon. The simulations show an extended feature above Great Britain with elevated NO concentrations of up to 80 pmol/mol. In this region aircraft emissions additionally contribute up to 70 pmol/mol to atmospheric background concentrations, suggesting that more than 40% of the total NO might originate from aircraft emissions. This day was subsequently chosen for a flight to detect

In situ observations of young contrails

C. Voigt et al.

Title Page

Abstract

Introduction

Conclusions

References

Tables

Figures



Back

Close

Full Screen / Esc

Printer-friendly Version

Interactive Discussion



aircraft NO corridor effects.

The region with enhanced NO was crossed twice by the Falcon on 31 October during a return flight from Oberpfaffenhofen to Shannon and back in the lowest stratosphere at altitudes between 10.5 and 11.6 km (Fig. 11). The detection of spikes in the NO and NO_y data within that region shows the presence of aircraft exhaust plumes with ages of minutes up to few hours (Schumann et al., 1998). The detection of aircraft plumes and their superposition is a first indication for the observation of aircraft corridor NO_x effects. In addition to the individual aircraft plumes, large scale elevated NO mixing ratios of 50 to 100 pmol/mol were detected in the lower stratosphere within the region influenced by the aircraft emissions compared to unperturbed stratospheric NO levels <50 pmol/mol. The measurements qualitatively agree with simulations with the MATCH-MPIC model of background and aircraft NO mixing ratios above Europe (Fig. 10). Hence we suggest that elevated NO levels in that region might be attributed to the superposition and dispersion of aged aircraft plumes and to regional aircraft NO effects. Our first rough analysis invites for a detailed study of the impact of aircraft NO in atmospheric composition. While several observations of the large scale NO_x impact of aircraft emissions in the upper troposphere exist (Schlager et al., 1997, 1999b; Ziereis et al., 1999; Schumann et al., 2000), our measurements are a rare case (Kondo et al., 1999; Koike et al., 2000) showing an extensive aircraft NO corridor effect in the lowermost stratosphere.

9 Detection of cirrus clouds

Cirrus clouds were observed during 10 CONCERT flights for almost 2 h detection time. The cirrus clouds were measured at temperatures between 213 and 246 K and at RHI of 126 to 54%, with more than 80% of the observations concentrating at RHI between 112 and 75% (see Fig. 3). Here we use the cirrus observations to show an instrument intercomparison of the CIP and the CPI, which were flown for the first time together on the same aircraft. In addition we show a water vapor instrument comparison of the

In situ observations of young contrails

C. Voigt et al.

Title Page

Abstract

Introduction

Conclusions

References

Tables

Figures

◀

▶

◀

▶

Back

Close

Full Screen / Esc

Printer-friendly Version

Interactive Discussion



frost point hygrometer and the Lyman α fluorescence instrument FISH.

9.1 Comparison of CPI and CIP measurements

Simultaneous measurements of the CPI (cloud particle imager) and the CIP (cloud imaging probe) have been performed on the flight on 20 November 2008 (Fig. 12). During that flight a mixed phase cloud has been detected during ascent. Further cirrus clouds as well as 3 contrails from a Fokker70, a B737 and an unknown aircraft have been observed at cruise. These contrails were embedded in cirrus clouds. The CIP was working during the first half of the flight. Therefore we show here the particle volume distribution within a cloud sequence detected during ascent. The particle volume distribution (Fig. 13) has been observed between 32 860 and 33 445 s UT above southern Germany. The cloud existed at altitudes between 4.3 to 8.7 km and a temperatures of 264 to 230 K. The particle size distribution in the particle size range of 80 to 400 μm shows a reasonable agreement between the two probes, still slightly lower particle concentrations were observed with the CPI compared to the CIP.

9.2 Water vapor comparison

The water vapor distribution in the troposphere and the lowest stratosphere was simultaneously probed with two instruments on the Falcon, the Lyman α fluorescence instrument FISH (Schiller et al., 2008) and a frost point hygrometer (Buck Research Instruments, LLC). Latter instrument was flown for the first time during the CONCERT campaign. The frost point hygrometer has been optimized during the campaign, therefore best agreement between the water vapor mixing ratios detected by the FISH instrument and the frost point hygrometer has been achieved on the last flight on 20 November shown in Fig. 12.

During this flight, the mean water vapor mixing ratio measured by the frost point mirror was 4% higher than the mixing ratio observed by the Lyman α instrument and lies within the errors of both instruments. The standard deviation of the ratio of the

Title Page

Abstract

Introduction

Conclusions

References

Tables

Figures

◀

▶

◀

▶

Back

Close

Full Screen / Esc

Printer-friendly Version

Interactive Discussion



5 significantly enhanced compared to background concentrations of $0.5 \mu\text{g m}^{-3}$ (Schmale et al., 2010). The increase of sulfate is most likely due to stratospheric OH-induced conversion of injected volcanic SO_2 leading to gaseous sulfuric acid, followed by condensation. The maximum SO_2 mole fractions of 510 pmol/mol in the plume very substantially exceed the atmospheric background SO_2 of about 40 pmol/mol (Jurkat et al., 2010). The ratio of particulate sulfate to total sulfur inside the plume was 0.8 ± 0.1 . From our measurements we conclude that the relatively large observed SO_2 mole fractions in the volcanic plume reflect slow OH-induced SO_2 conversion to sulfuric acid with an upper limit of the e-folding SO_2 lifetime of 60 days (Jurkat et al., 2010). This in turn reflects low OH in fall at high latitudes where the probed eruption plume parcel traveled mostly since the eruptions.

10 Additional trace gas measurements of HCl, HNO_3 and O_3 allow to investigate heterogeneous reactions taking place on the sulfate particles. The ratio HCl/ O_3 tends to be increased by 19% in the SO_2 -rich plumes compared to outside plume conditions suggesting direct injection of volcanic HCl into the stratosphere and very slow processing of HCl on the aerosol in the polar summer stratosphere. HNO_3/O_3 was enhanced by 50% in the plumes suggesting increased N_2O_5 hydrolysis on enhanced sulfate aerosols (Jurkat et al., 2010).

20 21% of the volcanic aerosol consisted of carbonaceous material, which is factor of 1.4 more than observed in UTLS background aerosol (Schmale et al., 2010). The increase of organic species may be due to direct injection of organic aerosol into the stratosphere. Alternatively, organic aerosol may form in the lower stratosphere from injected organic precursor gases, which became entrained into the tropospheric segment of the eruption column. The increased organic aerosol fraction might influence uptake coefficients and heterogeneous processing on volcanic sulfate aerosol.

25

**In situ observations
of young contrails**

C. Voigt et al.

Title Page

Abstract

Introduction

Conclusions

References

Tables

Figures

◀

▶

◀

▶

Back

Close

Full Screen / Esc

Printer-friendly Version

Interactive Discussion



11 Conclusions

Chemical, microphysical and radiative properties of contrails, cirrus clouds and volcanic aerosol were measured during the CONCERT campaign in October/November 2008 over Western Europe. The CONCERT particle data set provides a base for individual follow-up studies. Of particular interest is the first observation of the contrail from an A380-800 and the temporal evolution of particle size distribution and particle shape in the A380 contrail. Further the mixing of contrail ice crystals with ambient cirrus cloud particles and the evaporation of contrail ice crystals in ice sub-saturated conditions shall be addressed with model simulations. The data will be also be used to discuss the ratio between the volume mean and the effective radius of ice particles in cirrus clouds and contrails (Schumann et al., 2010). The contrail observations during the CONCERT campaign allow to investigate the impact of meteorological parameters as well as the impact of the aircraft type on radiative properties of young contrails.

In addition, the dependence of the fuel sulfur conversion efficiency ϵ_S and the HONO/NO ratio on the NO_x emission index of individual aircraft will be evaluated. Also the regional impact of aircraft NO_x emissions in the lowest stratosphere will be quantified and combined with detailed trajectory calculations.

The SO₂ lifetime in the polar lowest stratosphere can be derived based on measurements of the aged volcanic eruption plume from Mt. Kasatochi (Jurkat et al., 2010). Further, the detection of organic species in the aged volcanic aerosol layer (Schmale et al., 2010) should be investigated in sight of ozone modifications by heterogeneous processing of halogen and nitrogen species on volcanic aerosol.

Our extensive particle observations during the CONCERT campaign provide an unprecedented data set on particle size distributions, composition and trace gas fields in the mid-latitude tropopause region and their perturbation by aviation emissions, volcanic eruptions and cirrus clouds.

Acknowledgements. The CONCERT campaign was organized by the HGF-junior research group AEROTROP (Impact of Aircraft Emissions on the heterOgeneous chemistry of the

In situ observations of young contrails

C. Voigt et al.

Title Page

Abstract

Introduction

Conclusions

References

Tables

Figures

◀

▶

◀

▶

Back

Close

Full Screen / Esc

Printer-friendly Version

Interactive Discussion



TROPopause region). Part of this work was funded within the DLR-project CATS (Climate-compatible Air Transport System) and by the DFG SPP HALO 1294. We thank the DLR flight department for their excellent support during the campaign. A. Giez is gratefully acknowledged for his support with the calibration of the dewpoint hygrometer. ECMWF forecasts were provided in the context of the ECMWF Special Project: Support Tool for HALO Missions.

References

- Arnold, F., Scheid, J., Stilp, T., Schlager, H., and Reinhardt, M. E.: Measurements of jet aircraft emissions at cruise altitude I: the odd- nitrogen gases NO, NO₂, HNO₂ and HNO₃, *Geophys. Res. Lett.*, 19, 2421–2424, 1992. 12717, 12734
- Bonifacio, R.: METVIEW – Meteorological data visualisation and processing software at ECMWF, *ECMWF Newsletter* 86, Winter 1999/2000, 6–18, 1999. 12725
- Borrmann, S., Solomon, S., Dye, J., Baumgardner, D., Kelly, K., and Chan, K.: Heterogeneous reactions on stratospheric background aerosols, volcanic sulfuric acid droplets, and type I polar stratospheric clouds: Effects of temperature fluctuations and differences in particle phase, *J. Geophys. Res.*, 102(D3), 3639–3648, 1997. 12738
- Borrmann, S., Luo, B., and Mishchenko, M.: Application of the T-matrix method to the measurement of aspherical (ellipsoidal) particles with forward scattering optical particle counters, *J. Aerosol Sci.*, 31, 789–799, 2000. 12722
- Busen, R. and Schumann, U.: Visible contrail formation from fuels with different sulfur contents, *Geophys. Res. Lett.*, 22, 1357–1360, doi:10.1029/95GL01312, 1995. 12729
- Curtius, J., Sierau, B., Arnold, F., Baumann, R., Busen, R., Schulte, P., and Schumann, U.: First Direct Sulfuric Acid Detection in the Exhaust Plume of a Jet Aircraft in Flight, *Geophys. Res. Lett.*, 25(6), 923–926, doi:10.1029/98GL00512, 1998. 12733
- Curtius, J., Arnold, F., and Schulte, P.: Sulfuric acid measurements in the exhaust plume of a jet aircraft in flight: Implications for the sulfuric acid formation efficiency, *Geophys. Res. Lett.*, 29(7), 1113–1117, doi:10.1029/2001GL013813, 2002. 12735
- Canagaratna, M. R., Jayne, J. T., Jimenez, J. L., Allan, J. D., Alfarra, M. R., Zhang, Q., Onasch, T. B., Drewnick, F., Coe, H., Middlebrook, A., et al., Chemical and microphysical characterization of ambient aerosols with the aerodyne aerosol mass spectrometer, *Mass Spectrom. Rev.*, 26(2), 185–222, doi:10.1002/mas.20115, 2007. 12722

In situ observations of young contrails

C. Voigt et al.

Title Page

Abstract

Introduction

Conclusions

References

Tables

Figures

◀

▶

◀

▶

Back

Close

Full Screen / Esc

Printer-friendly Version

Interactive Discussion



**In situ observations
of young contrails**

C. Voigt et al.

Title Page

Abstract

Introduction

Conclusions

References

Tables

Figures

◀

▶

◀

▶

Back

Close

Full Screen / Esc

Printer-friendly Version

Interactive Discussion



- de Reus, M., Borrmann, S., Bansemer, A., Heymsfield, A. J., Weigel, R., Schiller, C., Mitev, V., Frey, W., Kunkel, D., Kürten, A., Curtius, J., Sitnikov, N. M., Ulanovsky, A., and Ravegnani, F.: Evidence for ice particles in the tropical stratosphere from in-situ measurements, *Atmos. Chem. Phys.*, 9, 6775–6792, doi:10.5194/acp-9-6775-2009, 2009. 12724
- 5 Drewnick, F., Hings, S. S., DeCarlo, P., Jayne, J. T., Gonin, M., Fuhrer, K., Weimer, S., Jimenez, J. L., Demerjian, K. L., Borrmann, S., et al.: A new time-of-flight aerosol mass spectrometer (TOF-AMS) – Instrument description and first field deployment, *Aerosol Sci. Technol.*, 39(7), 637–658, doi:10.1080/02786820500182040, 2005. 12722
- 10 Döpelheuer, A. und Lecht, M.: Influence of engine performance on emission characteristics, *Gas Turbine Engine Combustion, Emissions and Alternative Fuels*, Canada Communication Group. Inc., 1999. 12727, 12730
- Dürbeck, T. and Gerz, T.: Dispersion of aircraft exhausts in the free atmosphere, *J. Geophys. Res.*, 101, 26007–26015, 1996. 12728
- 15 Fahey, D. W., Eubank, C. S., Hubler, G., and Fehsenfeld, F. C.: Evaluation of a catalytic reduction technique for the measurement of total reactive odd-nitrogen NO_y in the atmosphere, *J. Atmos. Chem.*, 3, 435–468, 1985.
- Fahey, D. W., Keim, E. R., Boering, K. A., Brock, C. A., Wilson, J. C., Jonsson, H. H., Anthony, S., Hanisco, T. F., Wennberg, P. O., Miake-Lye, R. C., Salawitch, R. J., Louisnard, N., Woodbridge, E. L., Gao, R. S., Donnelly, S. G., Wamsley, R. C., Negro, L. A. D., Solomon, S., 20 Daube, B. C., Wofsy, S. C., Webster, C. R., May, R. D., Kelly, K. K., Loewenstein, M., and Podolske, J. R.: Emission Measurements of the Concorde Supersonic Aircraft in the Lower Stratosphere, *Science*, 270, 70–74, doi:10.1126/science.270.5233.70, 1995. 12733
- Febvre, G., Gayet, J.-F., Minikin, A., Schlager, H., Shcherbakov, V., Jourdan, O., Busen, R., Fiebig, M., Karcher, B., and Schumann, U.: On optical and microphysical characteristics of contrails and cirrus, *J. Geophys. Res.*, 114, D02204, doi:10.1029/2008JD010184, 2009. 25 12717
- Fiedler, V., Dal Maso, M., Boy, M., Aufmhoff, H., Hoffmann, J., Schuck, T., Birmili, W., Hanke, M., Uecker, J., Arnold, F., and Kulmala, M.: The contribution of sulphuric acid to atmospheric particle formation and growth: a comparison between boundary layers in Northern and Central Europe, *Atmos. Chem. Phys.*, 5, 1773–1785, doi:10.5194/acp-5-1773-2005, 2005. 12719
- 30 Fiedler, V., Nau, R., Ludmann, S., Arnold, F., Schlager, H., and Stohl, A.: East Asian SO_2 pollution plume over Europe – Part 1: Airborne trace gas measurements and source identification by particle dispersion model simulations, *Atmos. Chem. Phys.*, 9, 4717–4728,

**In situ observations
of young contrails**

C. Voigt et al.

[Title Page](#)[Abstract](#)[Introduction](#)[Conclusions](#)[References](#)[Tables](#)[Figures](#)[◀](#)[▶](#)[◀](#)[▶](#)[Back](#)[Close](#)[Full Screen / Esc](#)[Printer-friendly Version](#)[Interactive Discussion](#)

doi:10.5194/acp-9-4717-2009, 2009. 12719

Freudenthaler, V., Homburg, F., and Jäger, H.: Contrail observations by ground-based scanning Lidar: Cross-sectional growth, *Geophys. Res. Lett.*, 22, 3501–3504, 1995. 12716, 12717

Gao, R. S., Popp, P. J., Fahey, D. W., Marcy, T. P., Herman, R. L., Weinstock, E. M., Baumgardner, D., Garrett, T. J., Rosenlof, K. H., Thompson, T. L., Bui, T. P., Ridley, B. A., Wofsy, S. C., Toon, O. B., Tolbert, M. A., Kärcher, B., Peter, T., Hudson, P. K., Weinheimer, A. J., and Heymsfield, A. J.: Evidence that nitric acid increases relative humidity in low-temperature cirrus clouds, *Science*, 303, 516–520, 2004. 12717

Gayet, J.-F., Treffeisen, R., Helbig, A., Bareiss, J., Matsuki, A., Herber, A., and Schwarzenboeck, A.: On the onset of the ice phase in boundary layer Arctic clouds, *J. Geophys. Res.*, 114, D19201, doi:10.1029/2008JD011348, 2009. 12723

Heland, J., Kleffmann, J., Kurtenbach, R., and Wiesen, P.: A New Instrument To Measure Gaseous Nitrous Acid (HONO) in the Atmosphere, *Environ. Sci. Technol.*, 35, 3207–3212, doi:10.1021/es000303t, 2001. 12719

Heymsfield, A. J., Lawson, R. P., and Sachse, G. W.: Growth of ice crystals in a precipitating contrail, *Geophys. Res. Lett.*, 25, 1335–1338, 1998. 12717

Heymsfield, A. J.: On measurements of small ice particles in clouds, *Geophys. Res. Lett.*, 34, L23812, doi:10.1029/2007GL030951, 2007.

Holzäpfel, F.: Probabilistic Two-Phase Aircraft Wake- Vortex Model: Further Development and Assessment, *J. Aircraft*, 43, 700–708, 2006. 12730

Jurkat, T., Voigt, C., Arnold, F., Schlager, H., Aufmhoff, H., Schmale, J., Scheider, J., Lichtenstern, M., and Dörnbrack, A.: Airborne ITCIMS-measurements of SO₂, HCl, and HNO₃ in the aged stratospheric plume of volcano Mt. Kasatochi, *J. Geophys. Res.*, in review, 2010. 12719, 12738, 12739, 12740

Kärcher, B.: Aircraft-generated aerosols and visible contrails, *Geophys. Res. Lett.*, 23, 1933–1936, 1996. 12716, 12717

Kärcher, B., Hirschberg, M. M., and Fabian, P.: Small-scale chemical evolution of aircraft exhaust species at cruising altitudes, *J. Geophys. Res.*, 101, 15169–15190, 1996. 12734

Kärcher, B., Turco, R., Yu, F., Danilin, M., Weisenstein, D., Miake-Lye, R., and Busen, R.: A unified model for ultrafine aircraft particle emissions, *J. Geophys. Res. D: Atmospheres*, 105, 29379–29386, 2000.

Kärcher, B. and Voigt, C.: Formation of nitric acid/water ice particles in cirrus clouds, *Geophys. Res. Lett.*, 33, L08806, doi:10.1029/2006GL025927, 2006. 12717

**In situ observations
of young contrails**

C. Voigt et al.

Title Page

Abstract

Introduction

Conclusions

References

Tables

Figures

◀

▶

◀

▶

Back

Close

Full Screen / Esc

Printer-friendly Version

Interactive Discussion



- Kärcher, B. and Yu, F.: Role of aircraft soot emissions in contrail formation, *Geophys. Res. Lett.*, 36, L01804, doi:10.1029/2008GL036649, 2009. 12716, 12729
- Kärcher, B., Abbatt, J. P. D., Cox, R. A., Popp, P. J., and Voigt, C.: Trapping of trace gases by growing ice surfaces including surface-saturated adsorption, *J. Geophys. Res.*, 114, D13306, doi:10.1029/2009JD011857, 2009. 12717
- Koike, M., Kondo, Y., Ikeda, H., Gregory, G. L., Anderson, B. E., Sachse, G. W., Blake, D. R., Lib, S. C., Singh, H. B., Thompson, A. M., Kita, K., Zhao, Y., Sugita, T., Shetter, R. E., and Toriyama, N.: Impact of aircraft emissions on reactive nitrogen over the North Atlantic Flight Corridor region, *J. Geophys. Res.*, 105(D3), 3665–3677, 2000. 12736
- Kondo, Y., Koike, M., Ikeda, H., Anderson, B. E., Brunke, K. E., Zhao, Y., Kita, K., Sugita, T., Singh, H. B., Liu, S. C., Thompson, A., Gregory, G. L., Shetter, R., Sachse, G., Vay, S. A., Browell, E. V., and Mahoney, M. J.: Impact of aircraft emissions on NO_x in the lowermost stratosphere at northern midlatitudes, *Geophys. Res. Lett.*, 26, 3065–3068, 1999. 12736
- Kondo, Y., Toon, O. B., Irie, H., Gamblin, B., Koike, M., Takegawa, N., Tolbert, M. A., Hudson, P. K., Viggiano, A. A., Avallone, L. M., Hallar, A. G., Anderson, B. E., Sachse, G. W., Vay, S. A., Hunton, D. E., Ballenthin, J. O., and Miller, T. M.: Uptake of reactive nitrogen on cirrus cloud particles in the upper troposphere and lowermost stratosphere, *Geophys. Res. Lett.*, 30, 1154, doi:10.1029/2002GL016539, 2003.
- Konopka, P.: Analytical Gaussian solutions for anisotropic diffusion in a linear shear flow, *J. Non-Equilib. Thermodyn.*, 20, 78–91, 1995. 12728
- Krämer, M., Schiller, C., Voigt, C., Schlager, H., and Popp, P. J.: A climatological view of HNO₃ partitioning in cirrus clouds, *Q. J. Roy. Meteorol. Soc.*, 134, 905–912, 2008. 12717
- Lawrence, M. G., Rasch, P. J., von Kuhlmann, R., Williams, J., Fischer, H., de Reus, M., Lelieveld, J., Crutzen, P. J., Schultz, M., Stier, P., Huntrieser, H., Heland, J., Stohl, A., Forster, C., Elbern, H., Jakobs, H., and Dickerson, R. R.: Global chemical weather forecasts for field campaign planning: predictions and observations of large-scale features during MINOS, CONTRACE, and INDOEX, *Atmos. Chem. Phys.*, 3, 267–289, doi:10.5194/acp-3-267-2003, 2003. 12725, 12735
- Lee, D. S., Fahey, D. W., Forster, P. M., Newton, P. J., Wit, R. C. N., Lim, L. L., Owen, B., and Sausen, R.: Aviation and global climate change in the 21st century, *Atmos. Environ.*, 43, 3520–3537, doi:10.1016/j.atmosenv.2009.04.024, 2009. 12716
- Lewellen, D. C. and Lewellen, W. S.: The effects of aircraft wake dynamics on contrail development, *J. Atmos. Sci.*, 58, 390–406, 2001. 12716, 12731

- Meilinger, S. K., Kärcher, B., and Peter, Th.: Microphysics and heterogeneous chemistry in aircraft plumes – high sensitivity on local meteorology and atmospheric composition, *Atmos. Chem. Phys.*, 5, 533–545, doi:10.5194/acp-5-533-2005, 2005.
- 5 Miake-Lye, R., Anderson, B., Cofer, W., Wallio, H., Nowicki, G., Ballenthin, J., Hunton, D., Knighton, W., Miller, T., Seeley, J., and Viggiano, A.: SO_x oxidation and volatile aerosol in aircraft exhaust plumes depend on fuel sulfur content, *Geophys. Res. Lett.*, 25, 1677–1680, 1998. 12733
- Minnis, P., Schumann, U., Doelling, D. R., Gierens, K., and Fahey, D. W.: Global distribution of contrail radiative forcing, *Geophys. Res. Lett.*, 26, 1853–1856, 1999. 12716
- 10 Minnis, P., Palikonda, R., Walter, B. J., Ayers, J. K., and Mannstein, H.: Contrail properties over the eastern North Pacific from AVHRR data, *Meteorol. Z.*, 14, 515–523, 2005.
- Neuman, J. A., Gao, R. S., Fahey, D. W., Holecek, J. C., Ridley, B. A., Walega, J. G., Grahek, F. E., Richard, E. C., McElroy, C. T., Thompson, T. L., Elkins, J. W., Moore, F. L., and Ray, E. A.: In situ measurements of HNO₃, NO_y, NO, and O₃ in the lower stratosphere and upper troposphere, *Atmos. Environ.*, 35, 5789–5797, 2001.
- 15 Penner, J. E., Lister, D. H., Griggs, D. J., Dokken, D. J., and McFarland, M.: Aviation and the global atmosphere – A special report of IPCC working groups I and III. Intergovernmental Panel on Climate Change, Cambridge University Press, 365 pp., 1999. 12716
- Popp, P. J., Gao, R. S., Marcy, T. P., Fahey, D. W., Hudson, P. K., Thompson, T. L., Kärcher, B., Ridley, B. A., Weinheimer, A. J., Knapp, D. J., Montzka, D. D., Baumgardner, D., Garrett, T. J., Weinstock, E. M., Smith, J. B., Sayres, D. S., Pittman, J. V., Dhaniyala, S., Bui, T. P., and Mahoney, M. J.: Nitric acid uptake on subtropical cirrus cloud particles, *J. Geophys. Res.*, 109, D06302, doi:10.1029/2003JD004255, 2004. 12717
- 20 Schäuble, D., Voigt, C., Kärcher, B., Stock, P., Schlager, H., Krämer, M., Schiller, C., Bauer, R., Spelten, N., de Reus, M., Szakáll, M., Borrmann, S., Weers, U., and Peter, Th.: Airborne measurements of the nitric acid partitioning in persistent contrails, *Atmos. Chem. Phys.*, 9, 8189–8197, doi:10.5194/acp-9-8189-2009, 2009. 12717
- Schiller, C., Krämer, M., Afchine, A., Spelten, N., and Sitnikov, N.: Ice water content of Arctic, midlatitude, and tropical cirrus, *J. Geophys. Res.*, 113, D24208, doi:10.1029/2008JD010342, 2008. 12720, 12737
- 30 Schlager, H., Konopka, P., Schulte, P., Schumann, U., Ziereis, H., Arnold, F., Klemm, M., Hagen, D., Whitefield, P., and Ovarlez, J.: In situ observations of air traffic emission signatures in the North Atlantic flight corridor, *J. Geophys. Res.*, 102, D9, doi:10.1029/96JD03748, 1997.

**In situ observations
of young contrails**

C. Voigt et al.

Title Page

Abstract

Introduction

Conclusions

References

Tables

Figures

◀

▶

◀

▶

Back

Close

Full Screen / Esc

Printer-friendly Version

Interactive Discussion



12736

Schlager, H., Schulte, P., Flatoy, F., Slemr, F., van Velthoven, P., Ziereis, H., and Schumann, U.: Regional nitric oxide enhancements in the North Atlantic Flight corridor observed and modelled during POLINAT 2 – a case study, *Geophys. Res. Lett.*, 26, 20, 3061–3064, 1999.

12736

Schmale, J., Schneider, J., Jurkat, T., Voigt, C., Kalesse, H., Rautenhaus, M., Lichtenstern, M., Schlager, H., Ancellet, G., Arnold, F., Gerding, M., Mattis, I., Wendisch, M., and Borrmann, S.: Aerosol layers from the 2008 eruptions of Mt. Okmok and Mt. Kasatochi: In-situ UT/LS measurements of sulfate and organics over Europe, *J. Geophys. Res.*, doi:10.1029/2009JD013628, in press, 2010. 12722, 12738, 12739, 12740

Schmitt, A. and Brunner, B.: Emissions from aviation and their development over time, in: Pollutants from air traffic – results of atmospheric research 1992–1997, Final Report on the BMBF Verbundprogramm: Schadstoffe in der Luftfahrt, Tech. report, DLR – Mitteilung 97–04, pp. 1–301, 1997. 12735

Schröder, F., Kärcher, B., Duroure, C., Ström, J., Petzold, A., Gayet, J. F., Strauss, B., Wendling, P., and Borrmann, S.: On the transition of contrails into cirrus clouds, *J. Atmos. Sci.*, 57, 464–480, 2000. 12716, 12717, 12722, 12733

Schulte, P., Schlager, H., Ziereis, H., Schumann, U., Baughcum, S. L., and Deidewig, F.: NO_x emission indices of subsonic long-range jet aircraft at cruise altitude: In situ measurements and predictions, *J. Geophys. Res.*, 102 21431–21442, 1997. 12727

Schumann, U. and Konopka, P.: A simple estimate of the concentration beld in a flight corridor, in: Impact of Emissions from Aircraft and Spacecraft upon the Atmosphere. Proc. of an Intern. Sci. Colloquium, Köln (Cologne), Germany, 18–20 April 1994, edited by: Schumann, U. and Wurzel, D., DLR-Mitt. 94-06, Köln, Germany, 354–359, 1994. 12728

Schumann, U., Konopka, P., Baumann, R., Busen, R., Gerz, T., Schlager, H., Schulte, P., and Volkert, H.: Estimate of diffusion parameters of aircraft exhaust plumes near the tropopause from nitric oxide and turbulence measurements, *J. Geophys. Res.*, 100, 14147–14162, 1995. 12728, 12730

Schumann, U.: On conditions for contrail formation from aircraft exhaust, *Met. Zeit.*, 5, 4(23), 395–414, 1996. 12716, 12725, 12728, 12729

Schumann, U., Schlager, H., Arnold, F., Baumann, R., Haschberger, P., and Klemm, O.: Dilution of aircraft exhaust plumes at cruise altitudes, *Atmos. Environ.*, 32, 3097–3103, 1998. 12728, 12736

In situ observations of young contrails

C. Voigt et al.

Title Page

Abstract

Introduction

Conclusions

References

Tables

Figures

◀

▶

◀

▶

Back

Close

Full Screen / Esc

Printer-friendly Version

Interactive Discussion



**In situ observations
of young contrails**

C. Voigt et al.

[Title Page](#)[Abstract](#)[Introduction](#)[Conclusions](#)[References](#)[Tables](#)[Figures](#)[◀](#)[▶](#)[◀](#)[▶](#)[Back](#)[Close](#)[Full Screen / Esc](#)[Printer-friendly Version](#)[Interactive Discussion](#)

- Schumann, U., Schlager, H., Arnold, F., Ovarlez, J., Kelder, H., Hov, Ø., Hayman, G., Isaksen, I., Staehelin, J., and Whitefield, P.: Pollution from aircraft emissions in the North Atlantic flight corridor: Overview on the POLINAT projects, *J. Geophys. Res.*, 105(D3), 3605–3631, 2000. 12736
- 5 Schumann, U., Busen, R., and Plohr, M.: Experimental test of the influence of propulsion efficiency on contrail formation, *J. Aircraft*, 37, 1083–1087, 2000. 12716
- Schumann, U.: A contrail cirrus prediction tool, Intern. Conf. on Transport, Atmosphere and Climate, Aachen and Maastricht, 22–25 June 2009. 12728, 12729
- Schumann, U., Mayer, B., Graf, K., Mannstein, H., and Meerkotter, R.: A parametric radiative forcing model for cirrus and contrail cirrus, ESA Atmospheric Science Conference, Special Publication SP-676 (6 pages), Barcelona, Spain, 7–11 September 2009.
- 10 Schumann, U., Mayer, B., Gierens, K., Unterstrasser, S., Jessberger, P., Petzold, A., Voigt, C., and Gayet, J.-F.: Effective Radius of Ice Particles in Cirrus and Contrails, *J. Aeros. Sci.*, submitted, 2010. 12740
- 15 Starik, A., Savelév, A., Titova, N., and Schumann, U.: Modeling of sulfur gases and chemiions in aircraft engines, *Aerospace Sci. Technol.*, 6, 63–81, 2002. 12735
- Sussmann, R. and Gierens, K.: Lidar and numerical studies on the different evolution of vortex pair and secondary wake in young contrails, *J. Geophys. Res.*, 104, 2131–2142, 1999. 12716, 12731
- 20 Solomon, S., Portmann, R. W., Garcia, R. R., Randel, W., Wu, F., Nagatani, R., Gleason, J., Thomason, L., Poole, L. R., and McCormick, M. P.: Ozone depletion at mid-latitudes: Coupling of volcanic aerosols and temperature variability to anthropogenic chlorine, *Geophys. Res. Lett.*, 25, 1871–1874, 1998. 12738
- Somnitz, H., Gleitsmann, G. G., and Zellner, R.: Novel rates of OH induced sulfur oxidation. Implications to the plume chemistry of jet aircraft, *Met. Zeitschrift*, 14, 459–464, 2005. 12734
- 25 Speidel, M., Nau, R., Arnold, F., Schlager, H., and Stohl, A.: Sulfur dioxide measurements in the lower, middle and upper troposphere: Deployment of an aircraft-based chemical ionization mass spectrometer with permanent in-flight calibration, *Atmos. Environ.*, 41, 2427–2437, 2007. 12719
- 30 Stohl, A., Haimberger, L., Scheele, M. P., and Wernli, H.: An intercomparison of results from three trajectory models, *Meteorol. Appl.*, 8, 127–135, 2001. 12729
- Sussmann, R. and Gierens, K.: Lidar and numerical studies on the different evolution of vortex pair and secondary wake in young contrails, *J. Geophys. Res.*, 104, 2131–2142, 1999.

12716, 12731

Textor, C., Graf, H. F., Herzog, M., and Oberhuber, J. M.: Injection of gases into the stratosphere by explosive volcanic eruptions, *J. Geophys. Res.*, 108, 4606, doi:10.1029/2002JD002987, 2003. 12738

5 Tremmel, H. G., Schlager, H., Konopka, P., Schulte, P., Arnold, F., Klemm, M., and Droste-Franke, B.: Observations and model calculations of jet aircraft exhaust products at cruise altitude and inferred initial OH emissions, *J. Geophys. Res.*, 103, 10803–10816, 1998. 12717
Tompkins, A., Gierens, K., and Rädcl, G.: Ice supersaturation in the ECMWF Integrated Forecast System, *Q. J. Roy. Meteorol. Soc.*, 133, 53–63, doi:10.1002/qj.14, 2007. 12729

10 Unterstrasser, S., Gierens, K., and Spichtinger, P.: The evolution of contrail microphysics in the vortex phase, *Meteorol. Z.*, 17, 145–156, 2008. 12716

Unterstrasser, S. and Gierens, K.: Numerical simulations of contrail-to-cirrus transition – Part 1: An extensive parametric study, *Atmos. Chem. Phys.*, 10, 2017–2036, doi:10.5194/acp-10-2017-2010, 2010. 12731

15 Voigt, C., Schlager, H., Luo, B. P., Dörnbrack, A., Roiger, A., Stock, P., Curtius, J., Vössing, H., Borrmann, S., Davies, S., Konopka, P., Schiller, C., Shur, G., and Peter, T.: Nitric Acid Trihydrate (NAT) formation at low NAT supersaturation in Polar Stratospheric Clouds (PSCs), *Atmos. Chem. Phys.*, 5, 1371–1380, doi:10.5194/acp-5-1371-2005, 2005. 12720

Voigt, C., Schlager, H., Ziereis, H., Kärcher, B., Luo, B. P., Schiller, C., Krämer, M., Popp, P. J., Irie, H., and Kondo, Y.: Nitric acid in cirrus clouds, *Geophys. Res. Lett.*, 33, L05803, doi:10.1029/2005GL025159, 2006. 12717

20 Voigt, C., Kärcher, B., Schlager, H., Schiller, C., Krämer, M., de Reus, M., Vössing, H., Borrmann, S., and Mitev, V.: In-situ observations and modeling of small nitric acid-containing ice crystals, *Atmos. Chem. Phys.*, 7, 3373–3383, doi:10.5194/acp-7-3373-2007, 2007. 12720

25 Voigt, C., Schlager, H., Roiger, A., Stenke, A., de Reus, M., Borrmann, S., Jensen, E., Schiller, C., Konopka, P., and Sitnikov, N.: Detection of reactive nitrogen containing particles in the tropopause region – evidence for a tropical nitric acid trihydrate (NAT) belt, *Atmos. Chem. Phys.*, 8, 7421–7430, doi:10.5194/acp-8-7421-2008, 2008. 12717

Wendisch, M., Müller, D., Schell, D., and Heintzenberg, J.: An airborne spectral albedometer with active horizontal stabilization, *J. Atmos. Oceanic Technol.*, 18, 1856–1866, 2001. 12724
WMO (World Meteorological Organization): Scientific Assessment of Ozone Depletion: 2006, Global Ozone Monitoring Project – Report No. 50, 572., Geneva, Switzerland, 2007.

30 Wood, E., Herndon, S., Timko, M., Yelvington, P., and Miake-Lye, R.: Speciation and chemi-

ACPD

10, 12713–12763, 2010

In situ observations of young contrails

C. Voigt et al.

Title Page

Abstract

Introduction

Conclusions

References

Tables

Figures

◀

▶

◀

▶

Back

Close

Full Screen / Esc

Printer-friendly Version

Interactive Discussion



cal evolution of nitrogen oxides in aircraft exhaust near airports, Environ. Sci. Technol., 42, 1884–1891, 2008. 12734

Wormhoudt, J., Herndon, S., Yelvington, P., Miake-Lye, R., and Wey, C.: Nitrogen oxide (NO/NO₂/HONO) emissions measurements in aircraft exhausts, J. Prop. Power, 23, 906–911, 2007. 12734

Wernli, H. and Davies, H. C.: A Lagrangian-based analysis of extratropical cyclones. Part I: The method and some applications, Q. J. Roy. Meteorol. Soc., 123, 467–489, 1997. 12725

Ziereis, H., Schlager, H., Schulte, P., Köhler, I., Marquardt, R., and Feigl, C.: In situ measurements of the NO_x distribution and variability over the eastern North Atlantic, J. Geophys. Res., 104(D13), 16021–16032, 1999. 12736

Ziereis, H., Minikin, A., Schlager, H., Gayet, J. F., Auriol, F., Stock, P., Baehr, J., Petzold, A., Schumann, U., Weinheimer, A., Ridley, B., and Ström, J.: Uptake of reactive nitrogen on cirrus cloud particles during INCA, Geophys. Res. Lett., 31, L05115, doi: 10.1029/2003GL018794, 2004. 12720

Zöger, M., Afchine, A., Eicke, N., Gerhards, M. T., Klein, E., McKenna, D. S., Mörschel, U., Schmidt, U., Tan, V., Tuitjer, F., Woyke, T., and Schiller, C.: Fast in situ stratospheric hygrometers: A new family of balloon-borne and airborne Lyman- α photofragment fluorescence hygrometers, J. Geophys. Res., 104, 1807–1816, 1999. 12720

ACPD

10, 12713–12763, 2010

In situ observations of young contrails

C. Voigt et al.

Title Page

Abstract

Introduction

Conclusions

References

Tables

Figures

◀

▶

◀

▶

Back

Close

Full Screen / Esc

Printer-friendly Version

Interactive Discussion



In situ observations of young contrails

C. Voigt et al.

Title Page

Abstract

Introduction

Conclusions

References

Tables

Figures

◀

▶

◀

▶

Back

Close

Full Screen / Esc

Printer-friendly Version

Interactive Discussion

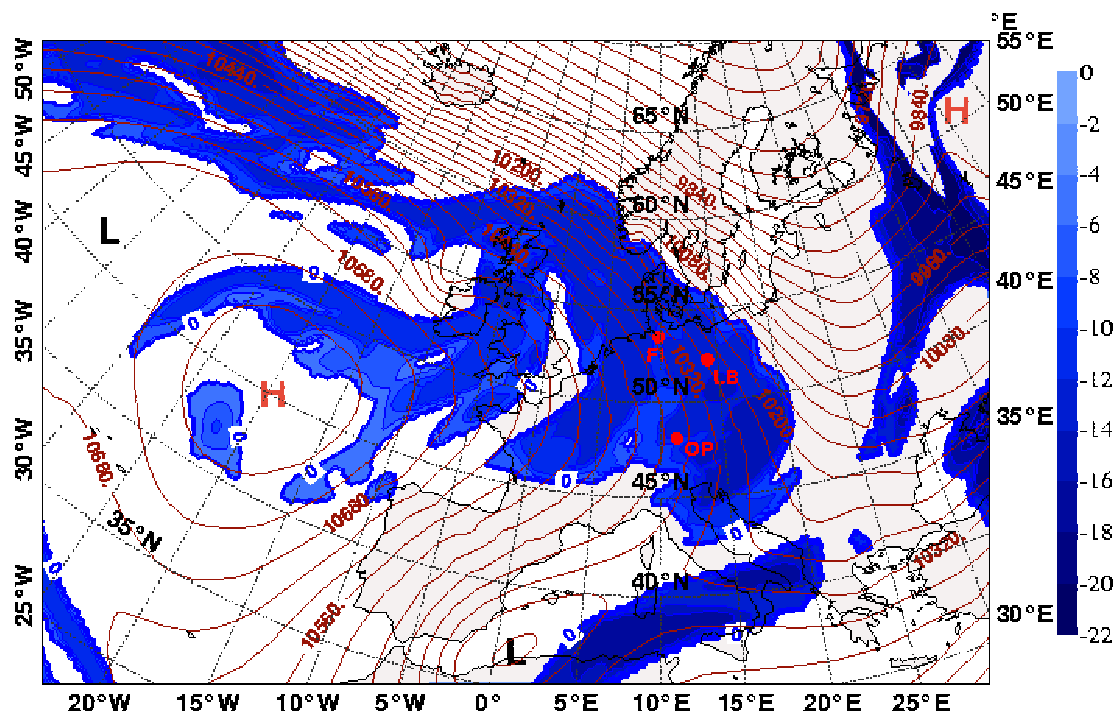


Fig. 1. 36 h forecast of the Schmidt-Appleman criterion at 250 hPa, valid on 19 November 12:00 UTC. Shown is the difference between the ambient temperature (K) as forecasted by the ECMWF and the threshold temperature for contrail formation as computed from the Schmidt-Appleman theory. Values are only plotted in regions where the relative humidity is larger than 80%, that is contrails that form in such a region have a high probability to be persistent. Red contours show the geopotential height (m).

In situ observations
of young contrails

C. Voigt et al.

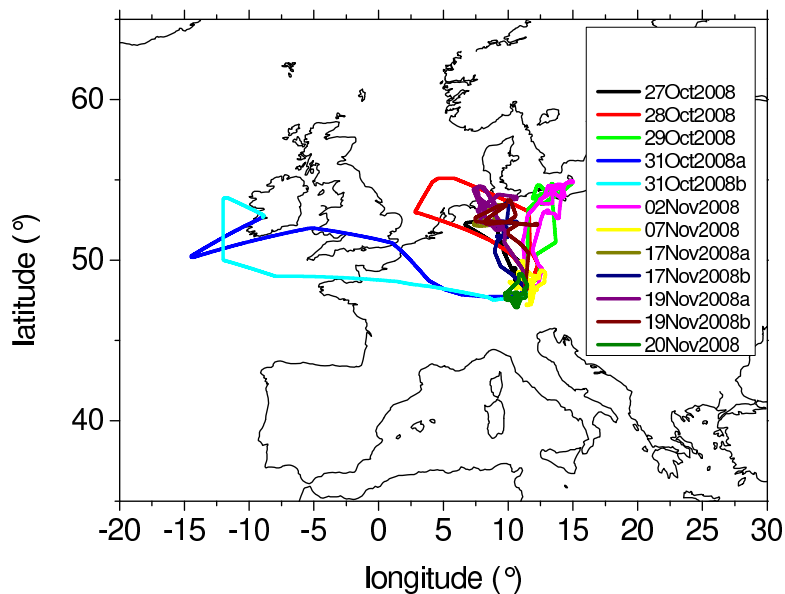


Fig. 2. Flight trajectories of 12 mission flights including 2 instrument test flights during the CONCERT campaign in October/November 2008 over Western Europe. The flight dates are given in the legend.

Title Page

Abstract

Introduction

Conclusions

References

Tables

Figures

◀

▶

◀

▶

Back

Close

Full Screen / Esc

Printer-friendly Version

Interactive Discussion



In situ observations
of young contrails

C. Voigt et al.

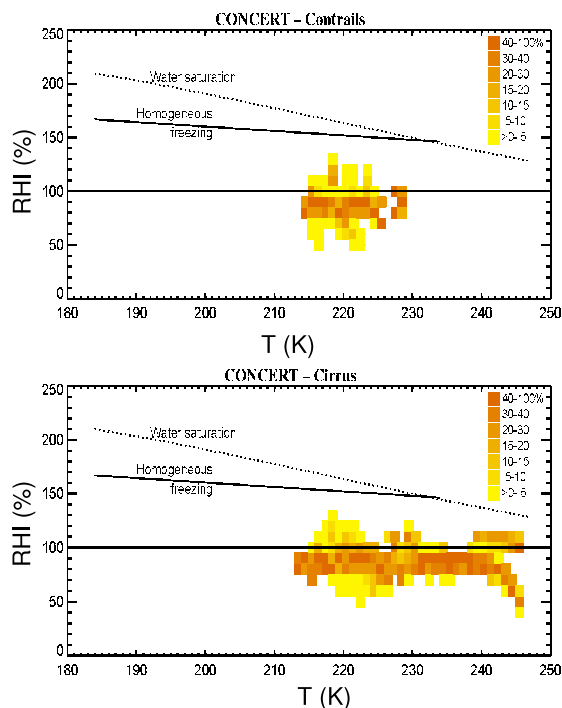


Fig. 3. Frequencies of occurrence of relative humidities over ice (RHI) versus temperature in contrails (upper panel) and cirrus clouds (lower panel) observed during the CONCERT campaign (thin solid line: homogeneous freezing threshold, dotted line: water saturation). The data are sorted in 1 K temperature bins. In each 1 K bin the sum of all data is 100%.

Title Page

Abstract

Introduction

Conclusions

References

Tables

Figures

◀

▶

◀

▶

Back

Close

Full Screen / Esc

Printer-friendly Version

Interactive Discussion



In situ observations
of young contrails

C. Voigt et al.

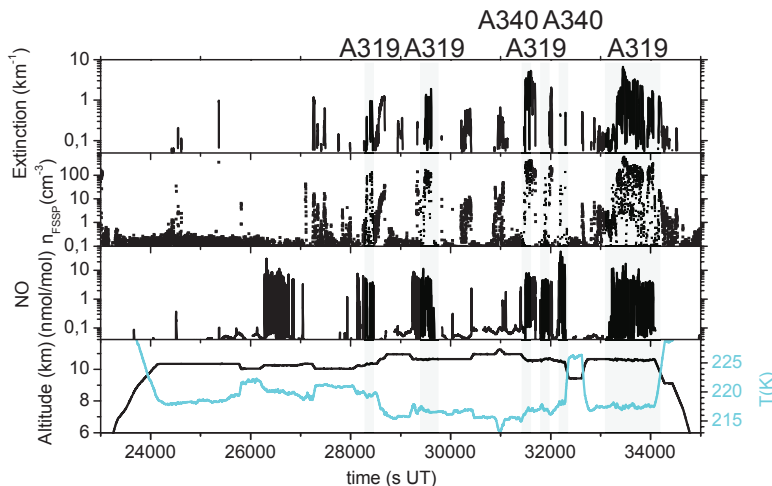


Fig. 4. Contrail flight A on 19 November 2008 above Germany from Oberpfaffenhofen to Hamburg. The flight altitude, temperature, RHI, and the NO mixing ratio as well as particle number density detected with the FSSP and the extinction are shown. Periodic gaps in the NO data are due to calibration events. Sequences of contrail encounters of an A319 and an A340 are marked in gray.

Title Page

Abstract

Introduction

Conclusions

References

Tables

Figures

◀

▶

◀

▶

Back

Close

Full Screen / Esc

Printer-friendly Version

Interactive Discussion



In situ observations
of young contrails

C. Voigt et al.

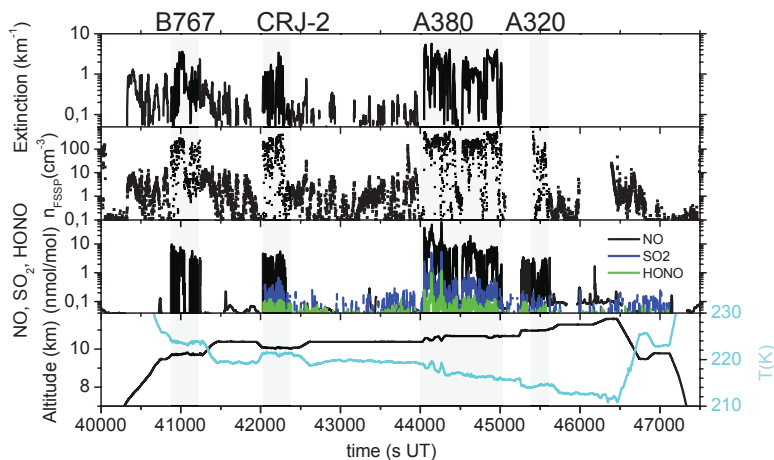


Fig. 5. Contrail flight B on 19 November 2008 above Germany from Hamburg to Oberpfaffenhofen. The flight altitude, temperature, RHI, and the NO, SO₂ and HONO mixing ratio as well as particle number density detected with the FSSP and the extinction are shown. Sequences of contrail encounters of a B767, a CRJ-2, an A380 and a A320 are marked in gray. Gaps in the NO, SO₂ and HONO mixing ratios are related to instrument calibrations. The PN stopped working at 45 050 s UT and there is a gap in the FSSP data between 45 050 s and 45 410 s UT.

Title Page

Abstract

Introduction

Conclusions

References

Tables

Figures

◀

▶

◀

▶

Back

Close

Full Screen / Esc

Printer-friendly Version

Interactive Discussion



**In situ observations
of young contrails**

C. Voigt et al.

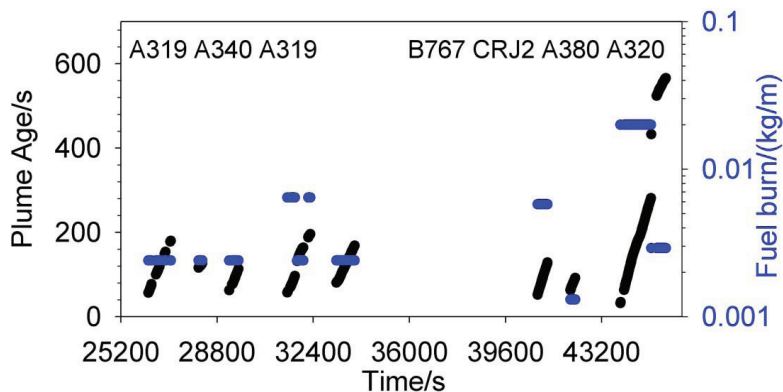


Fig. 6. Plume ages versus Falcon flight time and fuel consumption of the aircraft observed during two flights on 19 November 2008.

[Title Page](#)[Abstract](#)[Introduction](#)[Conclusions](#)[References](#)[Tables](#)[Figures](#)[◀](#)[▶](#)[◀](#)[▶](#)[Back](#)[Close](#)[Full Screen / Esc](#)[Printer-friendly Version](#)[Interactive Discussion](#)

In situ observations
of young contrails

C. Voigt et al.

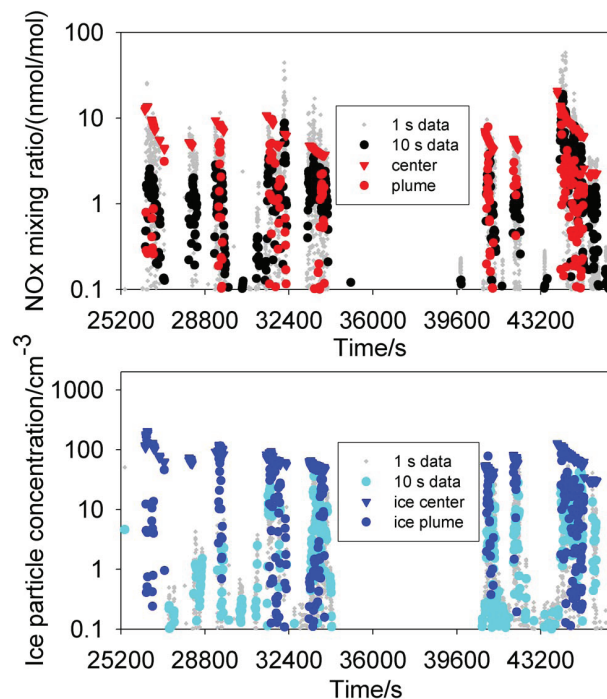


Fig. 7. Comparison of CoCiP model results to contrail observations during two flights on 19 November 2008. Upper panel: NO_x mixing ratio versus Falcon flight time. Measured data (grey and black dots) and computed results (red circles: along computed flight path; red triangles: on the plume axis). Lower Panel: Concentration of ice particles larger than $1 \mu\text{m}$ versus Falcon flight time. Measured data (grey and cyan dots) and computed results (blue circles: along computed flight path; blue triangles: on the plume axis).

[Title Page](#)[Abstract](#)[Introduction](#)[Conclusions](#)[References](#)[Tables](#)[Figures](#)[◀](#)[▶](#)[◀](#)[▶](#)[Back](#)[Close](#)[Full Screen / Esc](#)[Printer-friendly Version](#)[Interactive Discussion](#)

In situ observations
of young contrails

C. Voigt et al.

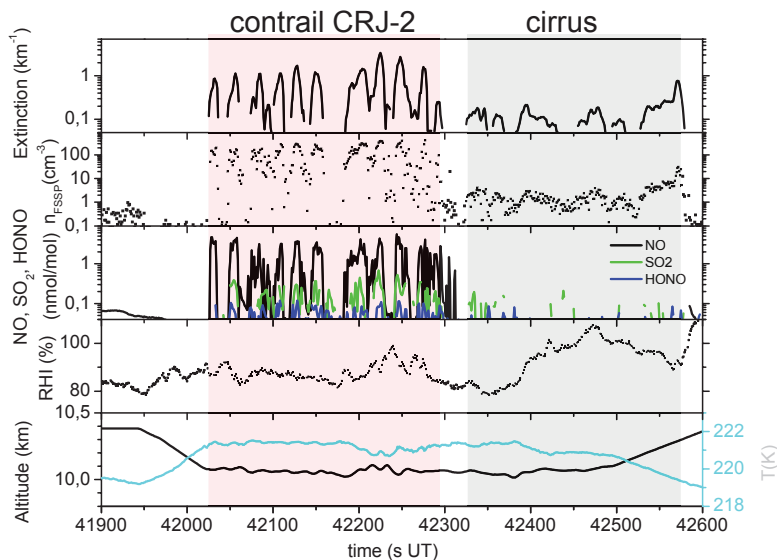


Fig. 8. Observations in the contrail from a CRJ-2 on 19 November 2008 above Germany. The flight altitude, temperature, RHI, and trace gas mixing ratios of NO, SO₂ and HONO as well as particle number density detected with the FSSP and extinction are shown. The contrail sequence is marked in red, cirrus encounters are marked in light gray.

Title Page

Abstract

Introduction

Conclusions

References

Tables

Figures

◀

▶

◀

▶

Back

Close

Full Screen / Esc

Printer-friendly Version

Interactive Discussion



In situ observations
of young contrails

C. Voigt et al.

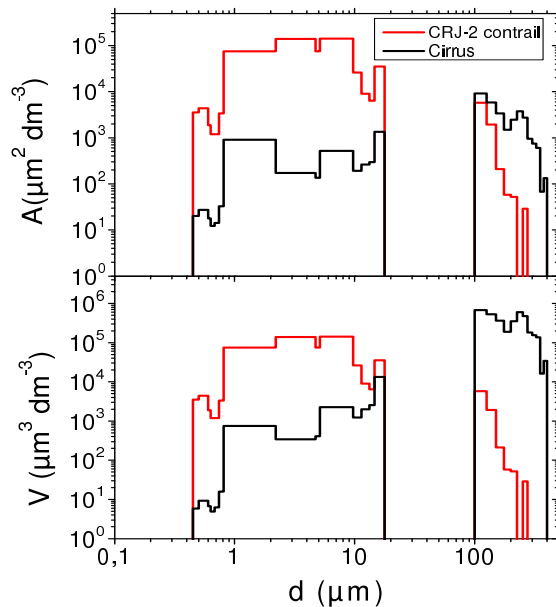


Fig. 9. Particle surface and volume distributions of the contrail from the CRJ-2 (red) embedded in a cirrus cloud (black).

[Title Page](#)[Abstract](#)[Introduction](#)[Conclusions](#)[References](#)[Tables](#)[Figures](#)[◀](#)[▶](#)[◀](#)[▶](#)[Back](#)[Close](#)[Full Screen / Esc](#)[Printer-friendly Version](#)[Interactive Discussion](#)

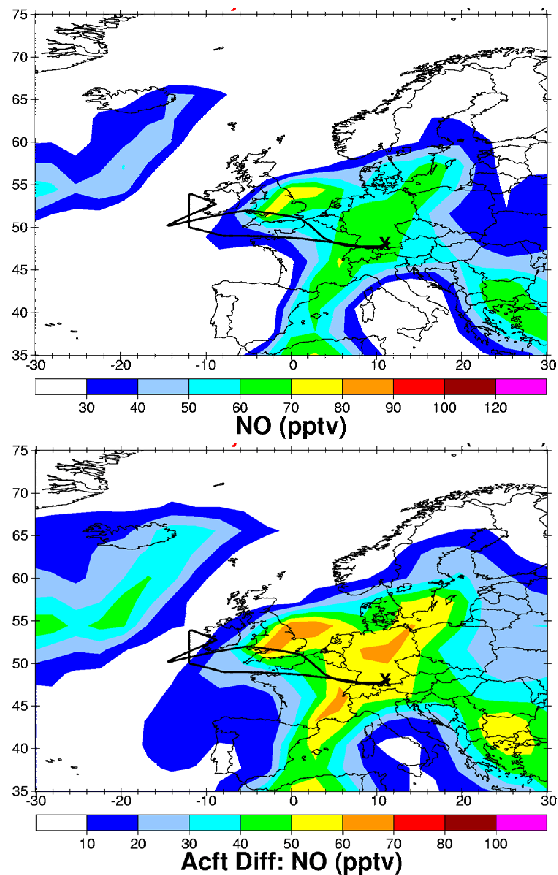


Fig. 10. Simulations with the MATCH-MPIC model of background NO (upper panel) and aircraft NO emissions (lower panel) on 31 October 2008, 12:00 UT, at 250 hPa above Europe.

**In situ observations
of young contrails**

C. Voigt et al.

Title Page

Abstract

Introduction

Conclusions

References

Tables

Figures

◀

▶

◀

▶

Back

Close

Full Screen / Esc

Printer-friendly Version

Interactive Discussion



In situ observations
of young contrails

C. Voigt et al.

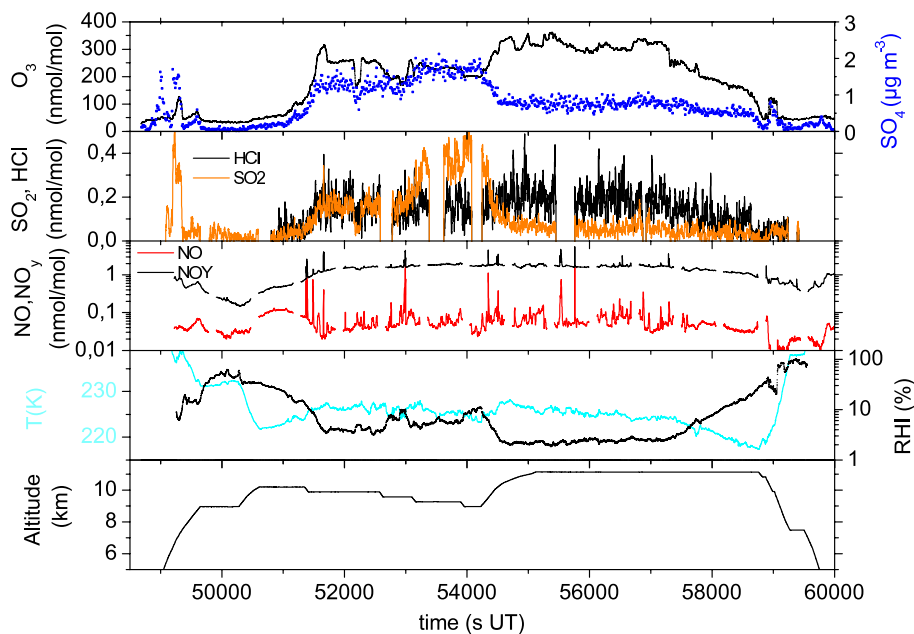


Fig. 11. Altitude, temperature, RHI, NO, NO_y , O_3 , SO_2 , HCl, and sulfate concentrations detected on 31 October 2008 on flight B from Shannon to Oberpfaffenhofen. Aircraft emissions in the lowest stratosphere and the aged eruption plume from volcano Mt. Kasatochi have been observed.

Title Page

Abstract

Introduction

Conclusions

References

Tables

Figures

◀

▶

◀

▶

Back

Close

Full Screen / Esc

Printer-friendly Version

Interactive Discussion



In situ observations
of young contrails

C. Voigt et al.

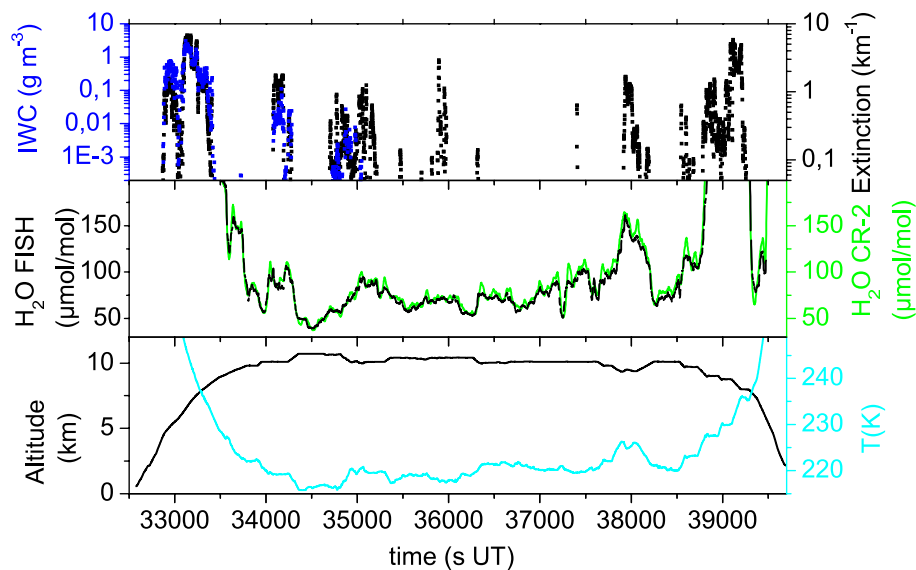


Fig. 12. Extinction, IWC, and water vapor mixing ratios detected with the frost point hygrometer and the Lyman α hygrometer onboard the Falcon on 20 November 2008. Also shown are flight altitude and temperature.

[Title Page](#)[Abstract](#)[Introduction](#)[Conclusions](#)[References](#)[Tables](#)[Figures](#)[◀](#)[▶](#)[◀](#)[▶](#)[Back](#)[Close](#)[Full Screen / Esc](#)[Printer-friendly Version](#)[Interactive Discussion](#)

**In situ observations
of young contrails**

C. Voigt et al.

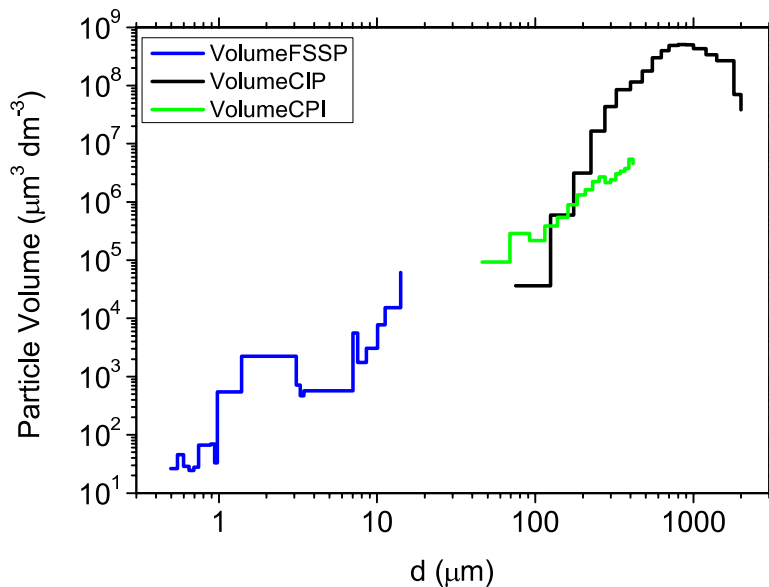


Fig. 13. Particle volume distributions of a cloud measured during ascent between 32 850 and 33 450 s UT on 20 November 2008 with the FSSP (blue) the CIP (green) and the CPI (black).

[Title Page](#)[Abstract](#)[Introduction](#)[Conclusions](#)[References](#)[Tables](#)[Figures](#)[◀](#)[▶](#)[◀](#)[▶](#)[Back](#)[Close](#)[Full Screen / Esc](#)[Printer-friendly Version](#)[Interactive Discussion](#)

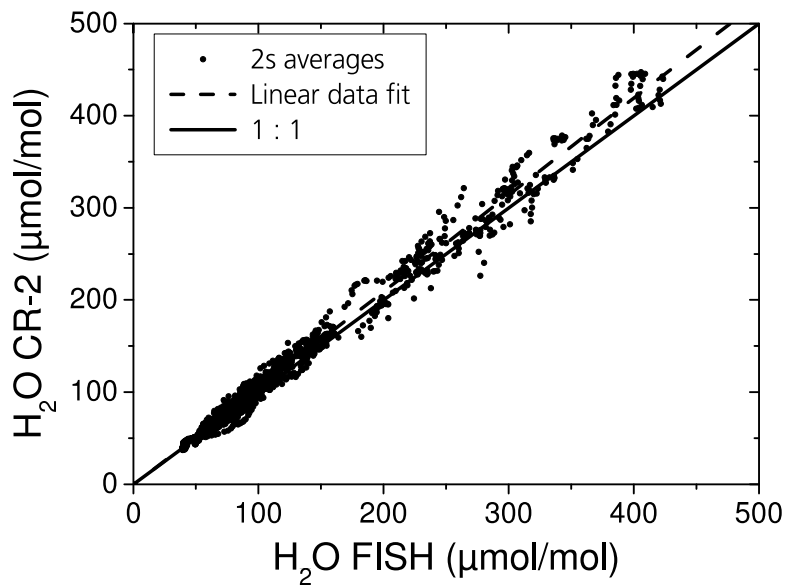


Fig. 14. Correlation between the water vapor mixing ratios detected with the frost point hygrometer and the Lyman α hygrometer. The 1:1 line and the linear regression are shown for illustration.

In situ observations of young contrails

C. Voigt et al.

Title Page	
Abstract	Introduction
Conclusions	References
Tables	Figures
◀	▶
◀	▶
Back	Close
Full Screen / Esc	
Printer-friendly Version	
Interactive Discussion	

